1. point-by-point response to all referee comments

Black: Comments from reviewers

Red: Answer from Authors

Green: Changes in manuscript

2. Author's reply to 'Review of wes-2020-31' by Anonymous Referee #1

Thank you very much for your detailed and valuable review of our manuscript. Below you find a copy of the referee's comments together with our responses marked in red.

3. Review of wes-2020-31

Overview

The manuscript, "Integrated wind farm layout and control optimization" submitted by Mads M. Pedersen and Gunner Chr. Larsen offers an analysis on wind plant layout and control optimization, finding that the two procedures may be treated separately without significant reductions to the benefits to AEP. The work decoupling the numerical operations offers some real potential to engineering processes for wind plant design and operation. However, the results lack generality and insufficient detail is provided on the means by which results are attained. The manuscript would be greatly strengthened by a discussion of whether the control and layout optimization steps can always be safely decoupled. This would help to simplify wind plant optimization in general, which is an NP-hard problem. In summary, the manuscript offers some results that have a potential benefit to the wind energy research community and industry, but more information is required before results can be confidently and generally reproduced.

It is correct, that it would greatly strengthen the generality of the manuscript if we could 'prove' that control and layout optimization can always be safely decoupled. This, however, implies that all possible generic integrated topology and wind farm control problems have this property - i.e. an arbitrary number of WTs, related arbitrary area constraints (i.e. WT 'density'), area shapes, wind climates etc. This is, unfortunately, not possible for this complex optimization problem, where an analytical solution providing such results are not possible.
This is also stated in the paper referring to the conclusion of Fathy et al., (2001): "A priory, it is not possible to evaluate whether the coupling between system design variables and system control variables is weak or strong for a complicated physical system like a WPP".

3.1. Major Comments

Wind plant control and operation by derating (i.e. axial induction control) is understood to be strongly dependent on the nature of the wake model used in wind plant performance modeling. No detail is provided on how wakes are modeled in the current work. Specifically, many well-known velocity deficit and wake-added turbulence models exist and provide different estimates on the benefits of pitch-based derating.

Rotors are modeled as actuator discs in a linear CFD framework - which in the paper is formulated as "The WTs are modelled as *actuator discs*, which in general can be vertically inhomogeneous, but often is assumed uniform". We will add that this model is used to model the wakes.
We are not modelling wake-added turbulence, as we are not considering WT loading but only WT production.

We have explicitly written that actuator disc model is used to model the wakes:

The optimization procedure is discussed only briefly and will probably not be well understood by researchers that are not already familiar with the methods. Consequently, reproduction or verification of the results will be virtually impossible by other groups.

We have added more details on the optimization procedure in the revised paper.

Finally, the layout optimization produces some results that do not seem to be appropriately constrained for implementation in reality, and may lead to overestimating the AEP gains. Turbines in the modeled wind plant appear to have been placed closer together than would be allowed in reality and in some cases are certainly operating in the near wake region of upstream turbines. Constraints or bounds on optimization parameters are not sufficiently clear in the manuscript.

The optimization is constrained by a minimum allowable distance to the nearest neighboring WT of 2D together with the convex boundary around the initial WPP layout. We will write this explicitly in section 2.4.

We have listed the optimization constraints, i.e. boundary, minimum spacing, pitch and rotor-speed limits in section 2.3

Page 1: Authors state that the procedure outlined in the manuscript is, “the fastest possible optimization procedure”. How is this determined? Can it actually be shown to be the fastest, or is it simply faster than a given alternative?

The point is that de-composed nested approach is much faster that the fully integrated optimization approach. We will reformulate this phrase.

We have replaced ”the fastest possible“ with “significantly faster”

Page 1: Increasing AEP for any wind plant by 4% is a very substantial change. Is this estimate derived by comparing a modeled baseline production to a modeled controlled case, or is power production reported by the SCADA system used at all. There is no discussion of the effects of turbulence on wind turbine wakes or wind plant performance anywhere in the paper. This is a crucial consideration for wind turbine wake interaction and mixing and plays a huge role in the outputs of wake models used for power estimation. How is turbulence considered in the modeling, optimization, or estimation of AEP?

Yes, 4% is a substantial change, but of the same order of magnitude as reported in other papers using different approaches. This result, however, is based on the assumption that the inflow to the wind farm is homogeneous, stationary and well-known. Furthermore, controller-specific constraints such as tower-exclusion zone and smooth transition between regions are not considered. We will state this in the manuscript.

We have state that controller-specific constraints and implementation issues are note considered

The 4% increase is relative to the model base line to obtain a consistent comparison. Comparing to SCADA data production would not make sense as model uncertainty then enter the 'equation'.

The effect of the ambient mean wind shear and turbulence characteristics on the wakes are specified in terms of a terrain roughness height, which in turn implicitly dictates the ambient turbulence conditions via the turbulence closure of the CFD model. We have included the applied roughness height and the turbulence intensity it dictates in the revised manuscript.

Page 5: “divergence free,” isn't this another way of stating “conservation of mass” for incompressible flows?

Yes. We will add this.

We have added “(i.e. conservation of mass),” after divergence free

Page 5: “linearity of the model, wakes from multiple upstream WTs can consistently be superimposed to construct the flow field further downstream”. How well do the authors expect this to reflect reality? From the governing equations, wake velocity deficits are highly non-linear. Other wake models use sum-of-squares superposition or maximum deficit approach. Why is a linear model assumed?

We use the linear sum because it is consistent with the linear perturbation expansion of the Navier-Stokes equations in Fuga. We expect it to be at least as good as conventional empirical engineering models for wake summation. Full-scale validation studies of Fuga shows good agreement between model predictions and reality. We will add references to these studies

We have added two references that compares Fuga simulations to full-scale measurements

Equations (2) and (3): These relationships are derived through model outputs of HAWCStab2 by artificially limiting the power coefficient for a fixed wind speed. Am I correct in reading that there is no anlytical or empirical relationship to describe the modified values of Cp and Ct? Is this why the authors use look-up tables?

Yes, it is correct. Based on outputs from HAWCStab2 (numerical simulations of the rotor aerodynamics based on rotor/blade aerodynamic characteristics and using the BEM (Blade Element Momentum) approach) for a range of rotor speeds and pitch angles, the relationship between Cp and Ct is found by finding the rotor speed and pitch angle that, for each value of Cp, result in the lowest possible Ct. This relation is stored in look-up tables.

Page 6: "The results shown in Figure 1 can be used for the entire range of mean wind speeds requested for the system optimization," Cp and Ct are both functions of wind speed as well. What makes the authors confident that that the results in Fig. 1 are applicable at wind speeds other than 8 m/s, where they were defined? Equations (2) and (3) clearly state that Cp and Ct are functions of the mean wind speed, conditioned on tip-speed ratio and blade pitch angle.

Thrust scales with U^2 and the thrust coefficient is normalized with U^2. Power scales with U^3 and the power coefficient is normalized with U^3. These relations, however, assumes that the deformation of the blades are not wind-speed dependent. In reality the static blade deformation depends on the wind speed – that is why Ct and Cp depends on U in equations (2) and (3). In this study we simplify the model by using the static rotor deformation corresponding to 8 m/s for all wind speeds, and we do not expect the optimization result to be significantly affected by this simplification. We will add this information to the manuscript. For a more general formulation (also mentioned in the paper as a potential possibility when describing the rotor aerodynamics using HAWC2Stab), where the dependence of the static rotor/tower deflection with mean wind speed is taken into account, the Ct and Cp results will have to be computed for each relevant mean wind speed.

We have added this explaination and argumentation in the manuscript

Equation (5): Define limits of integration, wind direction is not typically discussed in units of radians. Is a resolution of 1 m/s for the numerical integration sufficient to capture rapid changes in region 2?

We will replace radians with degrees.

We have replaced radians with degrees.

The plot below shows the change in AEP when increasing the wind speed resolution from 0.1 m/s to 2 m/s. It is seen that the "error" in AEP for a wind speed resolution of 1 m/s is less than 0.15%. We consider this accuracy sufficient, and we expect the error to be much lower when comparing two cases, which are both calculated with a resolution of 1 m/s.

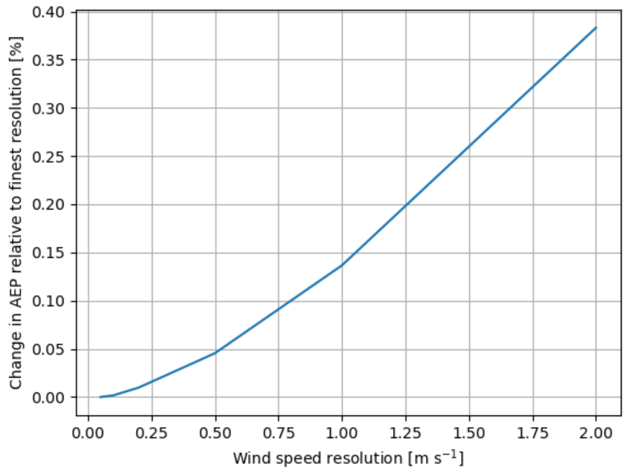

Figure 6, is the power production of each turbine relative to the nominal production at 8 m/s or is it relative to a different baseline value? Also, is the total power in Figure 7 just a sum of the plots in Figure 6?

Yes, both are correct, except that the power production refers to a mean wind speed equal to 10 m/s. We will clarify this in the manuscript.

We have stated that figure 6 referes to a mean wind speed of 10 m/s

Table 2: “Optimized Greedy 41.44 (+1.4%)” Results from 'sanity check' study indicate that optimal layout does not differ greatly from uniform spacing. Can the authors comment on the changes see in layout for case (2)? It also might be helpful to indicate computation time for each case, since that seems to be the justification for decoupling the layout and control optimizations.

The degree of freedom of the “sanity check”-example is limited to movement of the middle turbine. The result depends on the trends of of the power and thrust curves as well as the wind speed distribution. With the input used in this study, the optimal position is very close to the initial layout (equal spacing), and therefore only an infinitesimal increase is optained. In the 8-WT example, the optimizer has the freedom to move all turbines, and in this case the optimal layout is different from the initial layout. The plot below shows the cumulated AEP of the 8 WTs relative to the base line (i.e. initial layout and greedy control) as well as the position of the WTs (indicated by the dot markers). The green curve shows the optimal layout with greedy control (Case 2). It is seen that the distance between the two most upstream and the tree most downstream WTs are smaller than in the base case. This allows larger spacing and thereby production of the middle turbines, which, in this case, results in an increase of the AEP of the whole row. Obviuosly, this strategy is not possible with only three turbines.

We have extended the manuscript with an explaination of why the increase of case (2) is much higher than in the sanity check

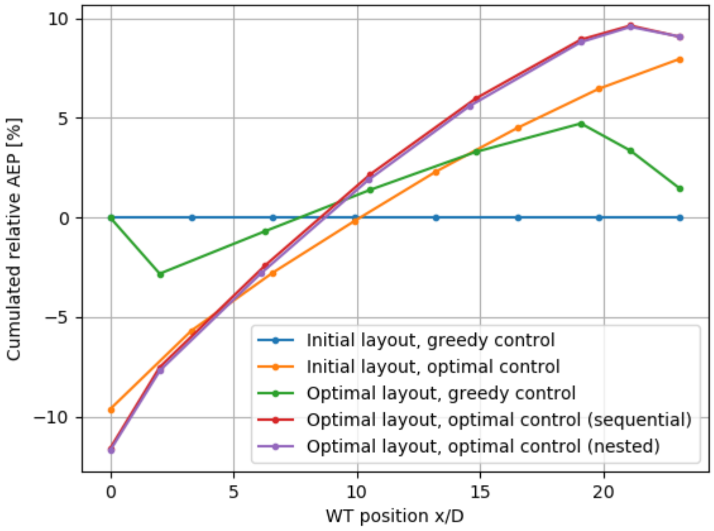

The computation time is indeed an argument for the decoupling. Otherwise, the problem solution for a WF of the Lillgrund size becomes a major computational challenge - even on a big cluster. The computation times for the 8-WT row are listed below and will be added to table 2 of the paper.

Case	Layout	Control	AEP [Gwh]	CPU time* [s]
0	Initial	Greedy	40.85	0.01
1	Initial	Optimized	44.10 (+8.0%)	4.20
2	Optimized	Greedy	41.44 (+1.4%)	2.84
3	Optimized	Optimized (sequential)	44.558	6.92
4	Optimized	Optimized (nested)	44.560	3731

* On standard laptop PC

We have added the computational time to the table

Figure 13: Note case(1) on the left and case(3) on the right. Also case(3) results do not seem intuitively correct. There appear to be areas where a wind turbine could be placed within the central area of the wind plant that would reduce the need to derate to the same extreme of 19%. How closely spaced are the wind turbines on the western and southeastern edges? Given that Lillgrund is already a tightly packed wind plant, these may be dangerously close or impractical. Are any bounds provided for wind turbine spacing? Is the same optimal layout used for all wind directions, or is layout different for each case?

Yes, we are using the same layout for all wind directions (as you cannot move WT when the wind direction changes), while the WT control settings varies with the wind direction.
The layout shown in Figure 13 is found to result in the highest overall AEP given the site conditions (wind speed distributions and wind direction frequency) used in this study. The inflow situation in Figure 13 reflects 10m/s from 223 deg, only, and for this particular flow case, the layout is obviously not optimal.
The optimizer places the WT very close on the western and south-eastern edges, but does not violate the 2D spacing constraint (indicated by the dashed circles)

3.2. Minor Comments

Throughout the manuscript:

Thank you very much for these comments. We will replace and rephrase as suggested.

We have addressed the minor comments in the revised manuscript

The naming convention of 'topology' is somewhat confusing. Suggest a change to WPP layout and WPP control, for clarity, as in the tables.

Commas and nested clauses are used with excess. For simplicity and readability, consider rephrasing with simpler, more direct messaging.

Phases are needlessly italicized throughout the text. Please remove text emphasis unless absolutely necessary.

Page 1: rephrase "in-stationary" as non-stationary or transient

Page 2: "A priory" -> a priori Page 2: rephrase, "and if so then how"

Page 3: rephrase as statement of research challenge rather than as a question. "Is it possible to conduct WPP system optimization based on a full-blown CDF simulation of the complex WPP flow field with its complicated WT wakes interactions?"

Page 4: "wind direction and -speed" -> "wind direction and wind speed"

Page 4: rephrase, "that is possible for at the requested"

Page 5: Rephrase "but often is assumed uniform" as "but is often assumed to be uniform in practice" or similar.

Figure 2: cut in wind speed for a SWT2.3-93 is 3.5 m/s

According to Siemens, there is no well-defined cut-in wind speed for the wind turbine used in the paper. In this study, we calculate the AEP based on power calculations for the wind speeds, 3, 4, ... , 25. In any case, the impact of the lowest wind speeds on the AEP are minimal and, in our opinion, insignificant for a layout study.

Page 8: "i.e. the WT position coordinates", are the coordinates (lat, long) the two design variables or is there another?

Yes, the two WT position design variables are the Cartesian x and y coordinates of the WT.

Page 8: "Both of the above-sketched optimization", Only a single optimization strategy has been show so far.

In the first strategy, all N(2+Nd Ns) design variables are optimized in one process, which is infeasible within the current frame work. The second strategy is the two-step nested approach. We will try to make this more clear in the manuscript.

We now use the names "one-step", "two-step nested", "two-step sequential" throughout the manuscript to make it easier to distinguish the three optimization strategies

Figure 4: caption should be on the same page as figure. Also consider making Figs 3 and 4 subfigures.

Use the \citet{} command for textual citations throughout the manuscript.

Page 9: How is the global optimum identified? In other words, how are the authors sure that the solution represents a global solution rather than a local optimum?

We cannot be sure that the presented solution is a global optimum, but we are confident that the result is close to optimal as we ran several long-run instances of the random search without getting a better result.

We have stated this in the manuscript

Table 1, insert comma after "layout"

Page 10: "both WT1 and WT2 is" -> "both WT1 and WT2 are"

Page 11: "the Cp- and the Ct dependence" -> "the dependence of Cp and the Ct on wind speed"

Figures 8 and 9: update vertical axis label. Simply writing "%" does not indicate what relative value is being considered.

Page 14: considerable -> considerably

Page 14: only insignificantly -> not significantly

Table 3: "4 Optimized Optimized(nested) -", remove from table if not pursued in analysis. Caption should be on same page as table

Page 15: analogue -> analogous

Page 15 "more than doubled compared to the" -> "more than double that of"

Page 17: “Introductory,” seems out of place.

4. 'Review of wes-2020-31', Anonymous Referee #2

4.1. Overview

“Integrated wind farm layout and control optimization”, written by Mads Pedersen and Gunner Larsen is generally well organized and well written. A wind farm layout and control optimization methodology is presented and analyzed. An approach to separating the control and layout optimizations is presented that is seemingly useful, but could use some further validation. The problem formulation is generally well presented, but could benefit from more detailed descriptions to make it easier for researchers to reproduce the results. There are a number of typographical and grammatical corrections that would improve the quality of the work, though none of them are extremely drastic. Finally, more discussion of the flow-field assumptions made may significantly reduce any doubt of the methods from the community.

4.2. High-level Comments

The use of two “example” studies to provide some intuition on the optimizing functions is a good way to tell the story, but the second example could provide more. By considering a single row of WTs, you are effectively removing a degree of freedom for the optimization solver to handle. It would be nice to see whether the AEP differences between the sequential and nested optimizations are still small for a minimal working example that doesn’t remove design variables, but just has a few turbines and an appropriately constrained space. This would help to remove any doubt that the sequential approach is sound.

We agree that a minimal example with two location degrees of freedom pr. WT would remove some doubt. To remove any doubt, however, the full example is required as the effects of both optimal layout and optimal derating is highly dependent on the number of turbines and the admissible site area and geometry. We have tried to optimize a minimal wind farm with 3x3 WTs, but the optimizer did not manage to find a trustworthy solution. We are therefore hesitating about adding such an example.

There is no mention or discussion of the wake model. This would be good to know more about, given that the proposed control method is axial induction control. Additionally, there is brief mention of the existence of wind shear and turbulence – details on this would be useful.

Rotors and wakes are modeled as actuator discs in a linear CFD framework - which in the paper is formulated as "The WTs are modelled as actuator discs, which in general can be vertically inhomogeneous, but often is assumed uniform". We will specify that this model is used to model the drag force, which in turn generates the wakes. The actuator disc's are modeled using the aerodynamic model described in detail in Section 2.2.

We have explicitly written that actuator disc model is used to model the drag force which in turn is responsible for creation of rotor downstream wakes

The effect of the ambient mean wind shear and turbulence characteristics on the wakes are specified in terms of a terrain roughness height, which in turn implicitly dictates the ambient turbulence conditions via the turbulence closure of the CFD model as based on Monin–Obukhov theory for neutral atmospheric stratification, which is assumed. We have included the applied roughness height and the turbulence intensity it dictates at WT hub height in the revised manuscript.

Especially because the optimized Lillgrund WPP has turbines that are so close together, some discussion of the validity of the linear CFD solver’s ability to accurately represent the near wake region of upstream turbines would be very helpful. This goes hand in hand with the need for a discussion on the wake model.

The linear CFD model does not rely on the assumption that the wind speed in the wake is U(1-2a) as e.g. the classical N.O. Jensen wake model. In principle, the wake model is therefore also valid in the near wake. The uniformly loaded actuator disc formulation, however, implies simplifications visible in the near wake region (no azimuthal or radial force variations etc.).

Some distance downstream the effect from such variations vanishes, and we expect the model prediction to be acceptable 2D downstream.

In the very beginning you note that "The purpose of this paper is to investigate the influence of optimal wind farm control on the wind farm layout". To me, the word influence feels misleading. If I am not mistaken, this work really is investigating the joint optimization of the layout and control, not specifically the influence of one on the other. It may be worth it to consider re-phrasing this, or restructuring the paper a bit make it clear that the influence is in fact being investigated.

You are right. We will change this formulation.

We have replaced "investigate influence of …" with "investigate the joint optimization of"

You briefly mention that the only location constraint is a minimum of 2D from the nearest WT and the wind farm boundaries. What motivated this distance? This (and any other constraints that exist) might better fit in the problem formulation, not in the conclusion.

The minimum-spacing constraint is applied to avoid the turbines to be placed unrealistically close together. The minimum distance of 2D is chosen because it is around the minimum distance we have seen in a real wind farm.

We will list the applied constraints in the problem formulation where it belongs.

We have listed the optimization constraints, i.e. boundary, minimum spacing, pitch and rotor-speed limits in section 2.3

The introduction offers a fairly good review of the relevant literature but could benefit from some revision and restructuring. There are a lot of sentences that are extended through a series of commas, semicolons, and dashes and can feel tedious.

We will review the introduction and try to make it easier to read

We have revised the introduction

The presentation of the use of a "detailed aero-servo-elastic model" for the optimization approach (P4.L26) is a bit of a stretch. It seems that the optimization itself uses simplified models (so-called "surrogates"), that are rooted in steady-state BEM solvers, but complete aero-elastic analysis is not done for the optimization. There certainly does not seem to be any dynamic "servo models", just the assumption that the employed individual WT controller is capable of perfectly tracking the derated Cp/Ct.

We are using the aero-servo-elastic tool HAWCStab2 with a detailed aero-elastic model of the turbine (i.e. no dynamic servos in the model) to establish a surrogate relationship between power and thrust. We will clarify this in the revised manuscript.

We have removed "servo" from the phrase

4.3. More detailed comments & formatting

Thank you very much for these comments, corrections and suggestions. We will replace and rephrase as suggested.

We have addressed the minor comments in the revised manuscript

In my opinion, the use of italics to emphasize words is over-used. Sometimes it is useful, but caused a little confusion for me at times as well.

There are a lot of leading and trailing hyphens that are unnecessary throughout.

P1.L10 – Should be clear that you are focused on controlling the turbines for wind-farm wide AEP maximization, not just doing standard wind turbine control. "A priori" is unnecessary in this sentence.

P1.L20 – "… the a Swedish offshore wind farm …"

P1.L19 – "…the capability ies of the developed …". Double check singular/plural adjectives throughout paper.

P1.L30 – "capital costs that depends on the WPP layout"

P2.L10 – "A priory" -> "A priori"

P3.L2 – modal or model?

P3.L10 – "tip speed ration"

P3.L22 – I'm not sure I see how this work is specifically "guided by" the statement in 2). Confusingly, you state that , 2) suggested that more "realistic" studies introduce a lot more uncertainty, and then you say that you are attempting to get more "realistic" results. I am admittedly not very familiar with the work in (Kheirabadi and Nagamune, 2019), so perhaps I am missing something here.

P3.L23 – "CDF" -> "CFD"

P3.L32 – "CDF" -> "CFD"

P4.L16 – "justifies"

P5.L23 – "relies on an extended"

P7.L4 – "(3, 10, and 15 m s^-1 are marked). The marking of the rotor speed limits is probably unnecessary and clutters the figure.

P7.L17 – "this is assured to the highest possible degree" – what do you mean by this?

P7.L17 – "implementation of the shortcuts"

P8.L18 – what do you mean by "both of the above … will eventually lead to the same result"? Only one of the optimization approaches is sketched "above"

P8.L1 – ".. there are three common ways…"

P9.L10 – "A few local optima" is vague. This statement should be elaborated upon and/or justified more.

Figure 4 – make sure the figure caption is on the same page as the figure

Figure 5 – what do the black up/down arrows represent?

Figure 6 – Having the axis derating percentages range from 0%-100%, but the power percentage range from 40% - 100% in the colorbar is confusing

Figures 8 and 9 – The titles on these two figures should probably be the same, or similar. At least the y-axis label, and perhaps the titles, should reflect the fact that the percentage value plotted is percent of relative power.

P14.L7 – "considerablye"

P14.L11 – case (4), a the (see major comments about my concerns with the lack of 2-D dimensionality in this second sanity check)

Table 3 – caption should be on same pages as table

P17.L10 – "Inherit" –> "inherent"

P17.L17 – "Introductory", This sentence is generally very confusing, and I am not sure I see the "clearly exaggeration

5.

SC1: **'Notes/questions on axial-induction based wake control / derating'**, **Pieter Gebraad**

Despite of successful field testing results of wake deflection (such as https://www.nrel.gov/docs/fy19osti/73991.pdf or https://www.wind-energsci.net/2/229/2017/), Pedersen and Larsen seem to come to the conclusion in their introduction that wake deflection is of smaller importance compared to wind turbine derating/axial induction based control. They refer to presentation slides from Andersen (2019) with LES studies, in addition to comparisons using low-fidelity models by Deshmukh.

We are not intentionally concluding that wake deflection is of smaller importance compared to wind turbine derating/axial induction based control: We are referring to Deshmukh and Allison (2017) who obtains 0.9% increase in AEP for wake deflection, 6.6% for wake expansion and propagation (axial induction control) and 17.7% when combining the two strategies.

It seems to me however that in the slides by Andersen (2019), also the power of the combination of turbines cannot be increased through turbine derating, see slide 13/16?

We are referring to Andersen (2019) who based on his two-turbine investigation finds that for a given reduction of the upstream WT thrust, the yaw wake deflection strategy is penalized more severely than the derating strategy measured in terms of aggregated power production of the two turbines analyzed in the study case. We will rephrase the sentence "The same conclusion was reached by Andersen (2019)" as this is not the case.

We have deleted the sentence "The same conclusion was reached by Andersen (2019)"

We are, however, arguing that axial induction control should not be rejected insignificant based on studies that uses either pitch regulation or rotor-speed regulation isolated, as a combination of pitch and rotor-speed regulation in most cases results in more power for the same level of thrust.

The plot below shows the thrust curves obtained with combined pitch and rotor-speed regulation (dashed lines) and with pitch regulation only (dotted lines). It is clearly seen that the combined pitch and rotor-speed regulation results in lower thrust for the same power production.

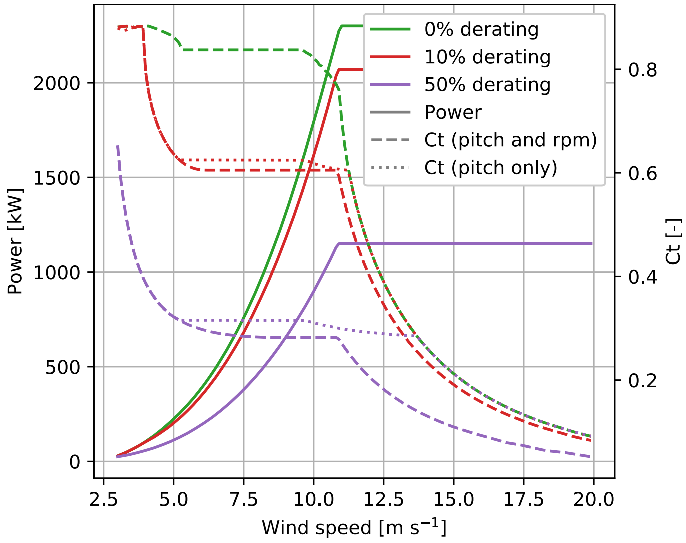

It is correct that slide 13 in Andersen (2019) does not show significant power gains for derating. According to the author, however, the derating strategy applied in this study is based on pitch regulation only. We therefore believe that this study do not reveal the full potential of derating.

The authors are referring to Gebraad, 2015 and mention that it is not taking into account the combination of pitch and TSR, thereby referring to Larsen's own work (Vitulli, 2019) where this was done. The combination of pitch and TSR is interesting, but it is questionable whether the linearized RANS modeling tool (FUGA) that was used by Vitulli can be used to compare results. The main points following out of Gebraad, 2015 and related publication (J. Annoni et al. Analysis of axial-induction-based wind plant control using an engineering and a high-order wind plant model. Wind Energy, 2015.), which was based on high-fidelity LES simulations using actuator-line rotors, are that when reducing thrust, also wake recovery is reduced because of reduced turbulence in the wake, limiting the potential of axial-induction based wake control. Secondly, when using pitch control in particular, the energy that is conserved in the wake is concentrated at the edge of the wake, so that most of that energy cannot be recovered at the downstream turbine. The linearized RANS modeling tool with actuator discs used in Vitulli's (and also now in Pedersen's work) might not be able to capture such effects? This is not to say that there could not be benefits of axial induction control, but it might be only applicable in very tightly spaced wind farms, and probably smaller than expected by the model used in Pedersen and Larsen.

It is also correct that Fuga, as well as all other models, are not able to capture all aspects of wake flow and WT interaction. In this case, however, simplifications of the flow field modeling is inescapable. It is simply not realistic to do wind farm layout and control optimization using a full non-linear LES coupled to meso-scale models for correct flow boundary conditions. Therefore, the question is how to simplify in the most adequate way. An alternative, widely used, simplification is to describe the wind-farm flow field by superposition of engineering/empirical single wake models. However, we consider the present direct solution to the wake affected wind farm flow field as an innovative, valid and competitive alternative to the traditional single-wake-based approach as it provides a consistent solution to the full set of linearized Navier-Stokes equations and thus avoids the challenging inconsistent merging of engineering single wakes into a wind farm flow field.

This is not to say that there could not be benefits of axial induction control, but it might be only applicable in very tightly spaced wind farms, and probably smaller than expected by the model used in Pedersen and Larsen. A recent paper (Effects of axial induction control on wind farm energy production-A field test, van der Hoek, 2019) shows benefits of axial induction control to be present, but smaller than expected from a CFD model (FarmFlow). The row production increase in below-rated conditions is reported to be 3.3%, while the spacing is more tight than the Lillgrund row where 8% increase in AEP was predicted by Pedersen and Larsen. Perhaps by recreating the scenarios, Pedersen and Larsen could have a critical look at their model's predictions compared to field testing results.

The mentioned recent paper (Effects of axial induction control on wind farm energy production-A field test, van der Hoek, 2019) is indeed interesting, and we will refer to it in our manuscript. Their FarmFlow simulations shows an increase of 5.6 %, which we consider in the same order of magnitude as our 8%. The numbers are, however, not directly comparable due to different turbine spacing, wind speed distributions, inclusion/exclusion of above-rated wind speeds and derating strategies (van der Hoek (2019) derates using pitch regulation only).

We have added references to this highly relevant study and related our findings to their results.

In the numerical study by van der Hoek (2019) as well as ours, the inflow field is assumed homogenous, stationary and well known. Furthermore, controller-technical and practical details such as tower exclusion zones and smooth transition between regions not are considered. In the field test by van der Hoek (2019), for instance, the derating is applied via a two-level pitch offset as the optimal pitch setting was too complicated to implement in the controller.
The power increase of 3.3% seen in the field test is therefore, in our opinion, surprisingly high compared to the simulation results. In any case, it confirms that the potential of axial induction control is worth to investigate.

6.

SC2**: 'Further discussion on axial induction based control', Pieter Gebraad**

-Yes, it seems that the combination of RPM and pitch is still interesting to still consider in axial-induction based wake control (perhaps mostly for closely spaced wind farms), as was discussed in earlier work "Optimal open loop wind farm control" by Vitulli.

We assert that for a given Cp contour, the intelligent choice of Ct is the smallest possible, because it results in the smallest/weakest possible wake. This is justified in our earlier work "Optimal open loop wind farm control", and can in general only be obtained using two design variables (pitch and rotational speed). The superiority of this strategy is in our opinion independent/unaffected of/by WT spacing - the weakest possible wake for fixed production is, in our opinion, always preferable from a wind farm production perspective.

I would still like to add some critical notes to your reply:
- Deshmukh and Alison used an early version of the FLORIS Multizone wake model with a FLORIDyn extension (aimed at modeling wake steering) for optimizing axial induction based control. This version of FLORIS/FLORIDyn Multizone has been shown to be inaccurate for optimizing axial-induction based control.

Thank you for the information about the inaccuracy of the FLORIS/FLORIDyn Multizone version used by Deshmukh and Alison (2017). This is of course unfortunate, but their paper has not been redrawn or updated, and we have not found public work that states that their conclusions are invalid, or that they are using an inaccurate FLORIS/FLORIDyn Multizone version. In fact, they do not mention FLORIS nor FLORIDyn in their paper. On this basis, we cannot dismiss their work as it is the only other study that combines layout and derating optimization as far as we know. We will, however, keep it in mind and not draw conclusions based on their work alone.

- Extensions to the FLORIS Multizone model are made in Annoni et al (DOI: 10.1002/we.1891) to match LES results with axial-induction based control, in which case the predicted benefit of axial induction based control disappears (at least if we use pitch control separately).

We had a look into the mentioned publication by Annoni et al (DOI: 10.1002/we.1891). With the 3.3% power increase, seen in the field study by van der Hoek (2019), in mind we find it strange that Annoni et al. finds no benefit of axial-induction-based control. The suggested empirical ad hoc modification of the basic Jensen top-hat model for turbines on a single row (fully overlapping wakes) is based on a fitting to SOWFA (CDF LES) simulations for one single ambient inflow speed (8m/s) and one ambient turbulence intensity (6%). For the investigated cases, the SOWFA simulations shows very little effect of the investigated de-rating cases. However, these are, as you correctly mention, obtained by adjusting the (collective) pitch setting only, which is sub-optimal (cf. the above comment on an optimal WT de-rating setting). The FLORIS-fitting is based on an adjustment of the Jensen expansion rate, which is argued to relate to the upstream WT axial induction parameter. It is difficult for us to follow the physical reasoning behind this relationship. We consider the downstream linear wake expansion assumption in the Jensen model to be primary dictated by wake meandering (cf. E. Machefaux et al. (2014). Empirical Modeling of Single Wake Advection and Expansion using Full Scale Pulsed Lidar based Measurements; WE) and consequently associated not only with turbulence intensity but also with turbulence structure (primary turbulence length scale). The paper by Annoni et al. clearly illustrates, that model simplifications comes with a price - more to this in the following.

- In your reply you state that Fuga is "not able to capture all aspects of wake flow and WT interaction", while in the paper, the model is advertised as a "full-blown CDF (sic.) simulation of the complex WPP flow field with its complicated WT wake interactions". There seems to be a mismatch in formulation. I think it would also be good to refer to the state-of-the-art in this field of research, where wake controls optimizations are in fact done with LES code (for example https://doi.org/10.3390/en11010177).

Perhaps this formulation about the capabilities of Fuga is unclear. What is really meant is that no model - including Fuga - is able to capture all aspects of wake flow and WT interaction. CFD LES is also an approximate approach, where the smaller scales are modelled, and where the precise interface to mesoscale flow boundary conditions is still an open question. Regarding the actuator line approach often used together with CFD LES simulations (also in SOWFA), work is still ongoing regarding the regularization kernel convolution of the blade forces (to avoid singularities in the numerical formulation), which also has an impact on WT power production (cf. recent work on Actuator-Line-Smearing-Correction by Alexander Meyer Forsting, Georg Pirrung and Néstor Ramos García; Wind Energ. Sci., 4, 369–383, 2019). Thus, high fidelity CFD simulation is not an unambiguous concept … and not necessarily the universal truth.
Fuga is a "full-blown CDF solver" in the sense that the solver consistently solves a set of first principles NS equations. This set is simplified as well as conventional CFD RANS and CFD LES are simplified, but it remains a "full-blown CDF solver".

Integrated wind farm layout and control optimization

Mads M. Pedersen[1], Gunner Chr. Larsen[1]

[1]Wind Energy Department, Technical University of Denmark, Frederiksborgvej 399, DK-4000 Roskilde, Denmark

Correspondence to: Mads M. Pedersen (mmpe@dtu.dk)

Abstract. ~~Design of an optimal wind farm topology and wind farm control scheduling depends on the chosen metric.~~ The objective of this paper is to investigate the ~~influence of optimal wind farm control on the optimal~~ joint optimization of wind farm layout and wind farm control in terms of power production. A successful fulfilment of this goal requires: 1) an accurate and fast flow model; 2) selection of the minimum set of design parameters that rules/governs the problem; and 3) selection of an optimization algorithm with good scaling properties.

For control of the individual wind farm turbines with the aim of wind farm production optimization, the two most obvious strategies are wake steering based on active wind turbine yaw control and wind turbine derating. The present investigation is ~~a priori~~ limited to wind turbine derating.

A high-speed linearized CFD RANS solver models the flow field and the crucial wind turbine wake interactions inside the wind farm. The actuator disk method is used to model the wind turbines, and utilizing an aerodynamic model, the design space of the optimization problem is reduced to only three variables per turbine – two geometric and one carefully selected variable specifying the individual wind turbine derating setting for each mean wind speed and direction.

The full design space spanned by these ($2N+N_d\,N_s\,N$) parameters, where N is the number of wind farm turbines, N_d is the number of direction bins, and N_s is the number of mean wind speed bins. This design space is decomposed in two subsets, which in turn define a nested set of optimization problems to achieve ~~the fastest possible~~a significantly faster optimization procedure compared to a direct optimization based on the full design space. Following a simplistic sanity check of the platform functionality regarding wind farm layout and control optimization, the ~~capabilities~~capability of the developed optimization platform is demonstrated on ~~the~~a Swedish offshore wind farm. For this particular wind farm, the analysis demonstrates that the expected annual energy production can be increased by 4% by integrating the wind farm control in the design of the wind farm layout, which is 1.2% higher than what is achieved by optimizing the layout only.

7. Introduction

The large-scale global deployment of wind energy is highly dependent on the cost of energy (COE), i.e. the profit of a wind power plant (WPP) over its lifetime as seen from an investor's perspective. Lowering the COE was previously addressed with the Topfarm WPP layout optimization platform (Réthoré et al., 2013; Larsen and Réthoré, 2013). The platform is used to design a WPP with minimal COE, for a given number of a predefined wind turbine (WT) type and an allowable area with an a priori known wind climate. Hence, it determines the optimal balance between WPP power production revenue on the one hand, and, on the other hand, all relevant expenses. The considered expenses include~~;~~: WPP variable capital costs (i.e. capital costs that ~~depends~~depend on the WPP layout); WPP operation and maintenance (O&M) costs, and cost of fatigue degradation of the individual components of all WTs in the WPP. The basic functionality of the Topfarm platform was later extended by also including the number of WPP WTs as a design variable, and the performance of surrogate models, needed to facilitate the used optimization algorithm, was moreover improved ~~(~~by Mahulja et al~~.,~~. (2018). Because WT loading is included, the WPP WTs must be modelled as aero-elastic models (including individual WT control), and the inflow conditions to these are tightly coupled to the complex ~~in~~non-stationary wake affected WPP flow field~~, which – for each iterative topology configuration – has to be simulated~~. Performing individual WT aero-elastic simulations for all the considered ambient wind speeds~~-~~ and wind directions~~. The optimization workflow – i.e. the iterative repetition of WPP flow field and corresponding aero-elastic~~

~~simulations   is~~ in each layout configuration iteration is extremely costly in terms of computational efforts~~, and the reason why~~. Therefore, surrogate models are needed to link ambient WPP inflow conditions, WT location within the WPP, and WT response in terms of power production and (fatigue) loading.

However, WPP control aspects were not considered in the aforementioned WPP layout optimization platform. Fathy et al., (2001) presents a pure theoretical analysis of coupled design and control of general physical systems. It was found that conventional sequential optimization processes are not guaranteed to find system-optimal designs. In this theoretical framework, a coupling term is introduced, which reflects the influence of plant dynamics/control on plant design. The necessary conditions for the combined plant design and controller optimality was investigated, and it was concluded that this term depends strictly on the gradients of the ~~coupling constraints~~couplings with respect to the plant design variables, which is also intuitively clear. Therefore, for weak/no coupling~~ –~~, i.e. neglectable coupling constraint gradients~~ –~~, the plant design and controller optimization problems become separable, and their sequential solution ~~will thus in turn furnish~~is equivalent to the combined optimum. In case of a strong coupling, only design methods that include this interaction explicitly can produce system-optimal designs contrary to the sequential approach. A ~~priory~~priori, however, it is not possible to evaluate whether the coupling between system~~-~~-design variables and system~~-~~-control variables is weak or strong for a complicated physical system like a WPP.

Fleming et al. (2016) and Gebraad et. al (2017) study optimization of layout and active wake control in terms of WT yaw dictated wake deflection on a WPP with 60 WTs. In these studies, the wake effects are modelled with an augmented version of the N. O. Jensen model (Jensen 1984) extended with an engineering model for wake deflection as caused by WT yaw misalignment. Fleming et al. (2016) consider an inflow wind speed of 8 m s^{-1}, only, and report a power gain of 2.3% for the optimized layout; 7.6% for the optimized yaw control; and 8.5% for the integrated layout and yaw control optimization result. ~~From the paper it is not clear whether power losses of yawed WTs are accounted for and if so then how.~~ Finally, Fleming et al. (2016) compares the integrated result, which requires 6900 CPU hours, with a sequential approach, which can be performed in "*several hours by a single computer*". They find that the integrated result is around 0.5% better than the results originating from the sequential approach. Gebraad et. al (2017) perform a three-step optimization: first the AEP is increased by 1.5% by optimizing the layout considering one wind speed per wind direction, only; then the WT positions and the yaw angle are optimized, again based on one wind speed per wind direction, which increases the AEP to 5.2% above the base line. Finally, the WT yaw angles are optimized for all relevant wind speeds raising the AEP to 5.3% above the base line.

Another integrated approach is taken ~~in (~~by Deshmukh and Allison~~,~~ (2017~~), in which the optimal layout of~~). They optimize a WPP system ~~is investigated~~ including ~~both~~ WPP ~~topology and~~layout as well as WPP control facilitated by active wake control over the entire lifetime of the WPP. The optimal WPP system design is pursued using a quasi-steady empirical wake model (i.e. a deterministic wake, which expands downstream). The quasi-steady wake model is linearly superimposed on the undisturbed ambient flow fields including both mean wind shear and turbulence (presumably using only one turbulence seed and thereby one realization of the ambient stochastic turbulence field) to obtain a description of the WPP flow field. Surprisingly, a relationship between the atmospheric boundary layer (ABL) turbulence field and the introduced wake expansion factor is not established, although there is evidence that wake meandering, which depends on the site ambient turbulence field, is dictating the static downstream wake 'envelope' (Machefaux et al., 2015). Deshmukh and Allison (2017) take a model predictive control (MPC) approach that is specifically implemented using reduced-order state-space models of the individual WTs, which account for the tower for-aft bending dynamics, the rotor rotational speed dynamics and the blade pitch dynamics. The active wake control includes both WT derating and wake deflection by WT yawing. The objective function is the WPP annual energy production (AEP), and two case studies indicate a significant improvement of the integrated system design compared to layout design only. No attempt was done to compare the full integrated system design approach with a sequential approach, in which first the layout was optimized and then, subsequently, the WPP control. Such a comparison would have contributed to quantification of the coupling terms, elaborated ~~on in (~~by Fathy et al~~.,~~. (2001), and, in case of weak coupling, facilitated a reduction the computational efforts needed to perform the system design optimization. The paper is ended with a comparison of the relative AEP effect of~~, respectively,~~ the derating and the yaw-wake-deflection strategy, respectively. It is concluded that wake deflection is of marginal importance compared to WT derating.

~~The same conclusion was reached by~~Based on a two-WT case, Andersen (2019) ~~based on a two-WT case~~ analyzed ~~in detail~~active wake control using a high-fidelity CFD LES solver, fully coupled with a modal-based aero-elastic tool including a full dynamic WT controller. Comparing a 35° yaw case with the corresponding derating case, this study concludes that, for a given reduction of the upstream WT thrust, the yaw wake deflection strategy ~~is penalized~~ reduces the power production of the upstream WT more ~~severely~~ than the derating strategy~~ measured in terms of aggregated power production of the investigated two-WT system.~~. It is further concluded that the overall benefit of active wake ~~control for a two-WT system~~deflection as well as WT derating is largely uncertain for a two-WT system.

~~This is opposite to the findings in~~ Gebraad et. al (2015~~). Like Andersen (2019), they~~) also analyzed a two-WT case by means of high-fidelity CFD simulations of the wind farm flow field coupled with simulations of the WT dynamics~~, using~~. They used the National Renewable Energy Laboratory's simulator for wind farm applications (SOWFA~~). Investigating~~) to investigate two different derating strategies~~—~~: 1) changing the collective blade pitch setting; and 2) changing the tip speed ~~ration — they~~ratio. They found ~~out,~~ that ~~what is gained by~~the power increase of the wake affected WT ~~is, on the whole, lost~~was balanced by the decrease of the derated WT. This lead to the conclusion~~,~~ that yaw wake deflection is more efficient than derating when quantified in terms of power production~~ gain~~. Unfortunately, both of the investigated derating strategies are sub-optimal as shown ~~in (~~by Vitulli et al. (2019). The optimal derating strategy is the particular combination of collective pitch- and tip speed setting ~~yielding~~resulting in the lowest rotor thrust for a given ~~derated~~WT power production. Using this optimal derating strategy, ~~considerable gains in power can be achieved as shown in (~~Vitulli et al. (2019~~).~~) obtained a considerable power gain.

Interestingly regarding both numerical two-WT studies by Andersen (2019) and Gebraad et. al (2015) is, in particular, a full-scale study by van der Hoek et al. (2019), in which derating of the most upstream WT was investigated for a single row of five WTs. Their CFD simulations predicted a power increase of 5.6% for the row-aligned wind direction in the below-rated wind speed regime. This result was verified by a year-long field test campaign, where WT derating was turned on and off every half week. The derating was, for practical reasons, implemented as two pitch offsets (one for full wake and one for partial wake conditions). The results of the field test predicted an increase of 3.3 % in AEP, i.e. close to the CFD simulations when taking the suboptimal pitch regulation as well as model and measurement uncertainties into account. Given that derating, based on pitch regulation only, is sub-optimal, there is a potential for even larger gain by using the optimal combination of pitch- and tip speed settings.

Large uncertainties, associated with both active wake control strategies (i.e. derating and yaw-based wake deflection) and, not least, among various simulation approaches as well as measurements, were also reported in (Kheirabadi and Nagamune, 2019). Important conclusions from this study is further, that 1) full-scale tests provide the most conservative (i.e. less optimistic) evaluations of the potential of active wake control; and consistently 2) "*added layers of realism in terms of simulated wind conditions tend to deteriorate the performance of wind farm controllers*".

Guided by 1) and 2), the present contribution to WPP system design optimization (i.e. WPP ~~topology~~layout- and control optimization) will seek to describe the complex inter-turbine aerodynamic interactions within a WPP as realistic as possible considering the computational resources needed for WPP optimization. This is done using ~~a~~an extremely fast full-blown ~~*CDF*~~CFD solver~~ in an attempt to get realistic results.~~ .

We will limit the scope to AEP[1] system optimization, ~~which is considered imperative for *direct* (~~i.e. ~~without the use of surrogates) use of CFD simulated WPP flow fields. In this context,~~ WT loading is excluded~~, and we consider, and will consequently~~. We assume~~,~~ that WT characteristics for aggregated AEP estimates are sufficiently described in terms of their power- and thrust coefficients, which implicitly include the relevant structural dynamics of a particular WT as e.g. crucial blade bending- and torsion dynamics for big modern WTs with flexible blades. ~~Based on~~Encouraged by the results obtained ~~in (~~by Deshmukh and Allison~~,~~ (2017~~;~~), Andersen~~,~~ (2019) and van der Hoek et al. (2019) we will ~~further concentrate on~~limit WPP active wake control ~~in terms of~~to WT derating and leave inclusion of yaw dictated wake deflection for a future study.

The research challenges dealt with in the present paper can be summarized as:

1) ~~Is it possible to conduct~~Investigate WPP system optimization based on ~~a~~ full-blown ~~CDF simulation~~CFD simulations of the complex WPP flow field with its complicated WT wakes interactions~~?~~;
2) Analyze and indicate the importance~~/size~~ of the system coupling terms mentioned in (Fathy, 2001) – or more specifically their gradients with respect to the WT positions; and
3) Evaluate the AEP improvement potential accompanying the integrated system approach with a focus on individual WT derating based on analysis of an existing offshore WPP.

Sect. 2 describes the simulation platform including all relevant models, while Sect. 3 presents a simple and illustrative application example as a sanity check. The Lillgrund case study is described in ~~Section~~Sect. 4. First the layout/control coupling is analyzed by a one-row WPP example. Based on the results of this study, a system optimization of the Lillgrund WPP is subsequently performed. The paper is concluded in ~~Section~~Sect. 5, where also future work is identified.

8. The platform

Overall, the integrated layout and WPP control optimization platform is based on a fusion of Topfarm2 (2019), the DTU wake framework, PyWake (2019), and a dedicated aerodynamic rotor model. Topfarm2, which is the DTU open source WPP optimization framework, utilizes the open-source framework for multidisciplinary design, analysis and optimization, OpenMDAO (Gray et al. 2019), to find the optimal set of design variables, i.e. WT positions and control settings in a sequential or nested workflow. PyWake is the DTU open source AEP calculator including a collection of stationary wake models. PyWake is used to establish the AEP objective function needed in Topfarm2, which in this study is based on the linearized CFD RANS wake model, Fuga (Ott et al. 2011).

A simplified version of the present platform, excluding WPP ~~topology~~layout optimization and thus only including WPP control optimization, is described ~~in (~~by Vitulli et al. (2019). In its most general formulation, this open-loop WPP control optimization platform deals with two design parameters per WT – the tip speed ratio, λ, and the collective pitch angle, α, both conditioned on the wind direction and ~~-~~wind speed. However, using a show case Vitulli et al. (2019) ~~justify~~justifies that the design space, without loss of generality, consistently can be collapsed to only one parameter for each WT. This parameter reflects the desired derating and maps to a unique combination of collective pitch and tip speed ratio, $(\alpha_{Ct}, \lambda_{Ct})$, which results in the smallest possible thrust coefficient, C_t, ~~that is possible for at~~ conditioned on the requested power coefficient, C_p. For the sake of efficiency, we will take advantage of this finding in designing the present platform, thus resulting in three design parameters for each WT – two ~~topology~~layout coordinates and the unique set $(\alpha_{Ct}, \lambda_{Ct})$ resulting from the unique functional relationship $\alpha_{Ct}(\lambda_{Ct})$.

In summary, the present integrated system optimization platform consist of four main components:

[1] Restricting the objective function to power production is a major simplification compared to approach taken in (Réthoré et al, 2013; Larsen and Réthoré, 2013; Mahulja et al., 2018) because: 1) aeroelastic modelling of the WPP WTs are circumvented; 2) a *stationary* description of the wake affected WPP flow field suffices; and 3) no cost models are needed.

1) A CFD solver modelling the steady flow field within a WPP. The ambient mean wind shear and turbulence characteristics are specified in terms of a terrain roughness height conditioned on wind direction, which ~~in turn~~ implicitly dictates the ambient turbulence conditions via the turbulence closure of the CFD model;
2) An aerodynamic part~~ that~~, which models the WT power- and thrust characteristics based on a detailed ~~aero-servo-elastic~~aeroelastic model of the WT~~, describing its~~. This model incorporates a description of both structural~~-~~ and aerodynamic properties ~~as well as the rotor~~ of the WT with predefined settings for rotational speed and the collective pitch angle~~. These are~~ conditioned on the rotor inflow conditions. However, only steady WT deflections is accounted for in defining the rotor aerodynamic characteristics for the present purpose. This model is in turn used to establish an accurate and fast surrogate model to facilitate an efficient optimization process;
3) A WPP AEP performance metric defining the optimization objective, including possible constraints, as based on a priori available information on the mean wind direction probability density function (pdf) and the mean wind speed pdf conditioned on the wind direction of the site; and
4) An optimization platform that computes the optimal system performance in terms of WPP AEP metric while satisfying the site area and minimum wind turbine separation constraints.

In the following each of these four key elements are described in some detail.

8.1. The CFD solver

Typically, an optimization of the control settings for a WPP requires 200 - 1000 power evaluations for each mean wind speed and ~~–~~direction. To calculate a proper AEP metric, we use 23 speeds and 360 directions; i.e. 1.6 – 8.2 million flow field computations is needed to optimize the control settings for a given WPP layout. Obviously, this puts excessively high demands on the computational speed of the flow solver.

The linear CFD RANS solver, Fuga (Ott et al., 2011), is extremely fast, has previously compared well with full-scale measurements (Peña et al. 2018, van der Laan et al. 2019), and is thus ~~appropriate~~considered ideal for this task. The governing Navier-Stokes equations, neglecting the Coriolis forcing, are consistently linearized using a formal perturbation expansion and subsequently retaining only the first order perturbation terms. Thus, mass conservation is identically satisfied, momentum conservation is satisfied to first order, and the resulting WPP fields are divergence free, as they should be for an assumed in-compressible flow. The resulting equations are in turn conveniently formulated and solved in a mixed-spectral domain for efficiency reasons. The velocity perturbation around a single WT in the physical domain is derived from Fourier components of the mixed-spectral solution using a fast inverse Fourier integral transform and stored in a system consisting of both general and WT-specific look-up tables, which facilitates the extreme computational speed of the solver. Because of the linearity of the model, wakes from multiple upstream WTs can consistently be superimposed to construct the flow field further downstream. From an efficiency perspective, this is a big advantage.

The WTs are modelled as actuator discs, which in general can be vertically inhomogeneous, but ~~often is assumed uniform.~~is often assumed uniform in wake studies. The actuator discs embedded in the flow field represent the rotor drag forces, which in turn is responsible for creation of rotor downstream wakes. The specifications of the individual actuator discs are based on detailed aerodynamic models of the WPP rotors as accounted for in Sect. 2.2. The WPP wind field, impinging at an arbitrary WT in the WPP, depends on the ambient wind field and wakes from relevant upstream WTs linearly superimposed. ~~The inflow conditions, i.e. mean wind speed and direction, are assumed spatially homogeneous.~~

The inflow conditions, i.e. mean wind speed and direction, are assumed horizontally homogeneous over the spatial extend of the WPP. More specifically, neutral atmospheric boundary conditions are assumed, meaning that a logarithmic mean wind shear profile applies. The characteristics of the shear profile is thus in turn defined by a terrain-roughness length and the friction velocity u_*. For neutral atmospheric conditions, Monin–Obukhov scaling dictates the standard deviation of the velocity fluctuations to be invariant through the atmospheric boundary layer and proportional to the friction velocity. The turbulence inflow is thus expressed in terms of the same input parameters as the mean wind shear field. For the Lillgrund site, a roughness length of z_0 = 0.03 m is used, which results in an inflow turbulence intensity of approximately 12%. This is in the high end for an offshore location and relates to the proximity of the Lillgrund site to urban areas. No attempt was done to link the roughness length to inflow wind speed, because site measurements have shown only marginal variations of the turbulence intensity with wind speeds below the rated wind speed.

For each wind direction, the local wind speed, i.e. ambient wind speed minus the sum of deficits from upstream turbines, the power production and the thrust coefficient as well as the wake deficits at downstream WT positions are evaluated starting with the most upstream WT position and continuing in the downstream order.

8.2. The aerodynamic WT model

As mentioned, we consider detailed aerodynamic rotor performance expressed in terms of power- and thrust coefficients as fully satisfactory for WT AEP simulations.

Initially, the power- and thrust coefficients of the rotor is modelled using HAWCStab2 – a linearized aero-servo-elastic code designed for stability analysis and steady-state simulation of WTs (Hansen et al., 2017). HAWCStab2 relies on an extended formulation of the traditional blade element momentum (BEM) approach (Madsen et al., 2007), and consequently detailed geometric- and aerodynamic input is required~~—~~, e.g. the blade planform and twist distribution as well as blade aerodynamic properties in terms of aerodynamic coefficients over the blade length. In the present application, HAWCStab2 uses a fully flexible WT model formulation to account for the equilibrium-static wind~~–~~-speed~~–~~-dependent deflections of the WT main components~~,~~ and thus the potential effects on the WT thrust- and power performance.

For traditional layout optimization without WPP control, the WPP production is implicitly based on WTs running at maximum C_p. For the present application, which aims at system optimal design, the aerodynamic modelling ~~must include~~includes a WT derating feature~~. As mentioned, this feature~~, which links to a unique set of tip speed ratio and collective pitch angle, (α_{Ct}, λ_{Ct}). Consequently, the aerodynamic WT model must facilitate computation of C_t and C_p conditioned on these design variables. Assuming zero yaw error, the tip speed ratio, λ, is defined as

$$\lambda \equiv \frac{R\Omega}{U} \tag{1}$$

where R is the rotor radius, Ω denotes the rotor speed, and U is the hub height mean wind speed.

The conditional dimensionless rotor thrust and power coefficients are defined as respectively

$$C_t(U|\alpha,\lambda) \equiv \frac{T_{WT}(U|\alpha,\lambda)}{½\rho A U^2} \tag{2}$$

and

$$C_p(U|\alpha,\lambda) \equiv \frac{P_{WT}(U|\alpha,\lambda)}{½\rho A U^3} \tag{3}$$

where T_{WT} is the rotor thrust force, P_{WT} is WT power production, ρ is the air density, and A is the rotor area, which depends on both the rotor tilt (θ_t) and the blade coning (θ_c) angles as

$$A = \pi(R\cos\theta_c \cos\theta_t)^2 \tag{4}$$

In this context, P_{WT} and T_{WT} is ~~the output~~obtained from HAWCStab2 simulations of the Siemens SWT-2.3-93 WT, which is operating at the Lillgrund WPP; see Sect. 10. The steady-state power and thrust have been simulated for a range of collective pitch and rotor-speed settings in a uniform flow field of 8 m s^{-1}. In principle such steady-state parameter sweep simulations must be performed for all relevant mean wind speeds to account for the steady-state blade deflections. However, assuming that these deflections have only a minor effect on the steady-state power and thrust performance for the WT in question, then one mean wind speed suffices. This is justified under the assumption that the thrust scales with U^2 and the thrust coefficient is normalized with U^2, whereas the power scales with U^3 and the power coefficient is normalized with U^3.

Note from eq. (1) that for a fixed wind speed, a variation in rotor speed corresponds to a variation of λ.

~~From these~~Thus, from the above described simulation outputs, the power- and thrust coefficients ~~have been~~are easily calculated as a function of the tip speed ratio and the collective pitch via equations (1) - (4); see Figure 1.

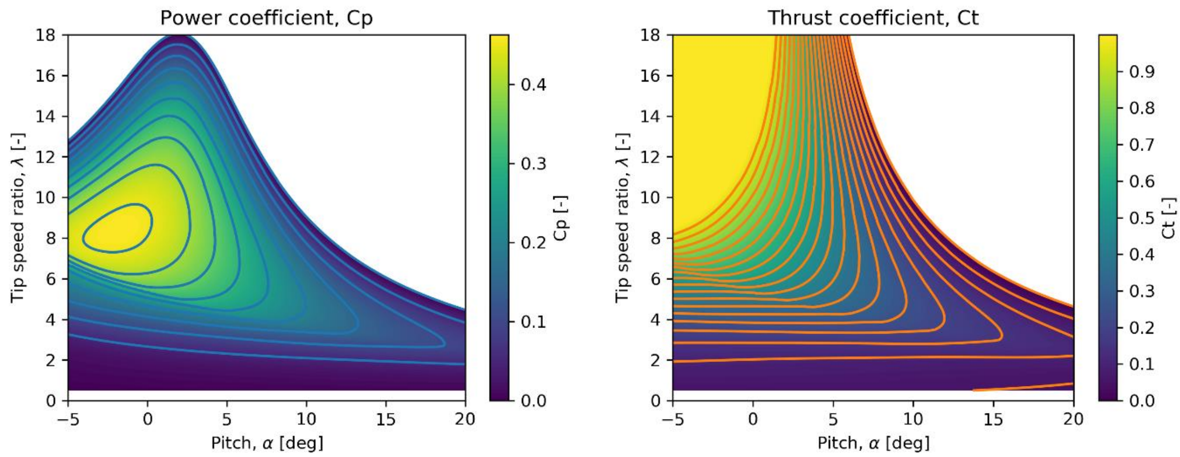

Figure 1. Power- and thrust coefficients as a function of tip speed ratio and collective pitch angle, based on HAWCStab2 simulations of a Siemens SWT-2.3-93 WT.

The results shown in Figure 1 can be used for the entire range of mean wind speeds requested for the system optimization, cf. eq. (1). This is convenient from a computational point of view, and thus consolidates the tip speed ratio as design variable as an appropriate choice.

Another important computational simplification is, as previously mentioned, the reduction from two~~-~~ control design variables per WT to one control design ~~variables~~variable per WT. This reduction is based on the previously mentioned findings ~~in (~~by Vitulli et al. (2019) showing that optimal derating is obtained by selecting the unique set of design variables, (α_{Ct} , λ_{Ct}) which, for a given derating (i.e. power production reduction), corresponds to the smallest possible thrust. This condition, which is also intuitively clear, provides a unique relationship between α_{Ct} and λ_{Ct} and justifies the reduction in design space to one control variable per WT, conditioned on ambient mean wind direction and ~~-~~mean wind speed.

As a consequence of the control design space collapse, a specific derating factor corresponds to a deterministic path through the original (α , λ) design space, where the points on this path correspond to certain mean wind speeds. Note, that these paths are constrained by the minimum and maximum rotor speed limits as well as the maximum power limit, see Figure 2.

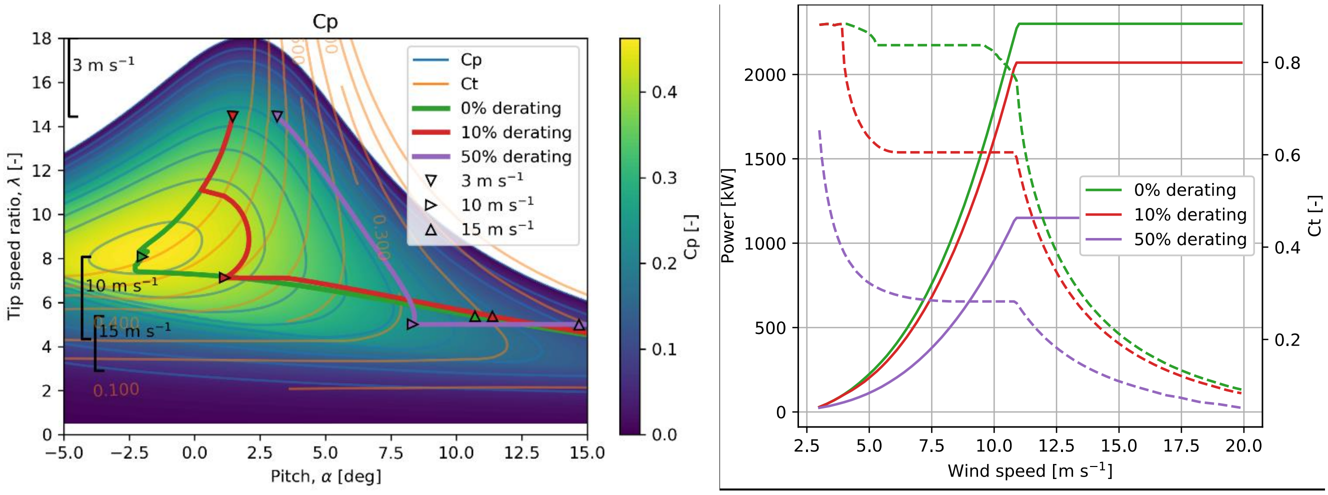

Figure 2. Left: C_p, (background colour and blue contours) and C_t (orange contours) plotted as a function of tip speed ratio, λ, and collective pitch setting, α. The green, red and purple lines expose the (α_{Ct}, λ_{Ct})-relation for 0%, 10% and 50% derating, ~~repectively~~respectively. These relations are plotted for a range of wind speeds (3, 10 and 15 m s^{-1} is marked) satisfying the rotor speed limits (indicated in the left-hand side of the figure for 3, 10 and 15 m s^{-1}) as well as the maximum power limit. Right: The corresponding power (solid) and C_t (dashed) curves plotted as a function of wind speed. These figures are based on HAWCStab2 simulations of a Siemens SWT-2.3-93 WT model.

The last step needed to prepare for an efficient optimization procedure is to transform the above described aerodynamic rotor computations into a surrogate model, which maps mean hub wind speed and the requested derating factor into a power production- and a thrust coefficient conditioned on the operational settings; i.e. $C_p\,(U\,|\,\alpha\,,\lambda)$ and $C_t\,(U\,|\,\alpha\,,\lambda)$. The surrogate thereby establishes the link between the derating settings, to be specified by the control optimizer, and the characteristics of the uniformly loaded actuator discs needed by the flow solver. Note, that controller-specific constraints such as tower-exclusion zone and smooth transition between regions as well as controller implementation issues are not taken into account. At present, it was not found essential to model the actuator discs as vertically in-homogeneous, although possible within the framework.

8.3. The AEP performance metric and constraints

The objective function defined for the present optimization platform is the AEP of the WPP. Financial costs of internal WPP power grid etc. are not considered, which in turn means that the positions of the individual WPP WTs are only constrained by the minimum allowable distance to the nearest neighboring WT and the line of demarcation defining the permissible WPP area. Considering 2 rotor diameters (*D*s) to be the minimum realistically WT interspacing distance, this minimum spacing constraint has been selected for all show cases presented in this paper. The permissible WPP area for the Lillgrund case is the stylized convex shape of the Lillgrund reef. Finally, we have incorporated additional two constraints associated with the operational conditions of the Lillgrund Siemens SWT-2.3-93 WT used in all cases: $\Omega \in$ [9 rpm; 16 rpm] and $\alpha \in$ [-2°; 90°].

In each iteration of the optimization procedure, the objective function – in this case the AEP performance metric – must be computed. Computational efficiency is in particular needed for the present CFD-based approach, and ~~this~~maximum efficiency is assured ~~to the highest possible degree~~ through implementation of the 'shortcuts' described in ~~section~~Sect. 2.2.

For a given ~~*topology*~~layout (i.e. associated with a given iterative step in the ~~topology~~layout optimization process), the WPP AEP, P_{AEP}, is estimated from

$$\cancel{P_{AEP} = T\sum_{i=1}^{N}\int_{0}^{2\pi}\int_{U_{in}}^{U_{out}} P_i(U|\theta) f_U(U|\theta) f_\theta(\theta) dU d\theta}\; P_{AEP} = T\sum_{i=1}^{N}\int_{0^\circ}^{360^\circ}\int_{U_{in}}^{U_{out}} P_i(U|\theta) f_U(U|\theta) f_\theta(\theta) dU d\theta \quad (5)$$

in which U denotes the undisturbed ambient hub-height mean wind speed and $P_i(U|\Theta)$ is the production (in watt) of the i^{th} WT at ambient hub-height mean wind speed, U, and associated operating conditions dictated by the internal WPP flow field. $f_U(U|\Theta)$ is the ambient hub-height mean wind speed pdf, conditioned on the ambient mean wind direction (i.e. often a two parameter Weibull distribution), and $f_\Theta(\Theta)$ is the ambient mean wind direction pdf. Assuming SI units, T is the number of seconds corresponding to one year, and N is the pre-defined number of WTs within the WPP considered.

In practice, eq. (5) is discretized to facilitate evaluation of the involved integrals. In the succeeding study cases, a directional discretization of 1° was used combined with an ambient mean wind speed discretization of 1 m s^{-1}.

8.4. Optimization setup

Overall, there is three common ways to design the WPP system optimization. The most elaborate of these is to design the full integrated approach by involving all design variables simultaneously~~.~~ - the *one-step* approach. The ~~topology~~layout optimization related design variables amount to two (i.e. the WT position ~~coordinates~~in a Cartesian coordinate system) per WT. The WPP control optimization, conditioned on ambient mean wind direction and mean wind speed, requires, utilizing the design space collapse described in ~~section~~Sect. 2.2, one design variable per WT. However, because the AEP computation requires all wind directions and all wind speeds to be accounted for, the control-related design variables amounts to $N_d\,N_s$ per WT. Here N_d is the number of ambient inflow directions, and N_s is the number of ambient mean wind speeds considered in the discrete version of eq. (5). Thus, in total the number of design variables amounts to $N(2+N_d\,N_s)$. This is clearly infeasible within the present framework – even when utilising a high-performance-computing cluster.

An alternative and more efficient strategy for a full integrated system optimization is a *two-step nested* approach, in which, for each optimization step, first the ~~topology~~layout is advanced and then, based on this iteration of the ~~topology~~layout, the associated optimal control schedule, conditioned on ambient mean wind speed and direction, is determined. Merging the sequentially determined ~~topology~~WPP layout and associated optimal control schedule, the AEP estimate, associated with the actual iterative step, can be evaluated. The associated workflow is illustrated in Figure 3.

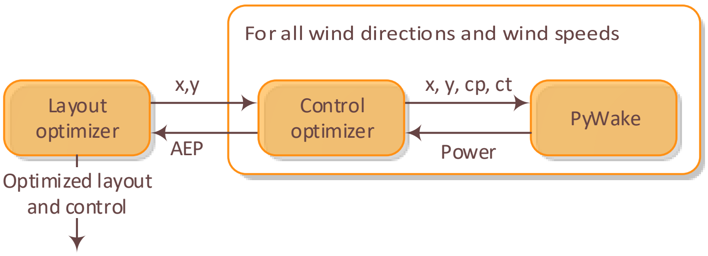

Figure 3. Nested optimization workflow. The control settings are optimized in every layout iteration.

Both ~~of~~ the ~~above-sketched~~one-step optimization ~~strategies~~strategy and the two-step nested optimization strategy are fully integrated strategies, which eventually will lead to the same result.

If the optimal system design is separable, in the sense that only a weak coupling exists between the ~~topology~~layout- and the WPP control optimization, the problem can be significantly simplified. This will be quantified in ~~section~~Sect. 9.3 and ~~section~~Sect. 10.1 using two demonstration cases. The significant reduction in computational complexity is obtained taking a *two-step sequential* approach by approximating a weak system coupling with no system coupling. The sequential workflow, in which the conventional ‘greedy’ individual WT control settings are used for the WPP layout optimization, is succeeded by an optimization of the WPP control scheduling conditioned on both ambient mean wind speed and direction. Thereby, the ‘greedy’ WT control settings are replaced by optimized ‘collaborative’ WT settings to the benefit of the WPP AEP. The workflow associated with this sequential strategy is shown in Figure 4.

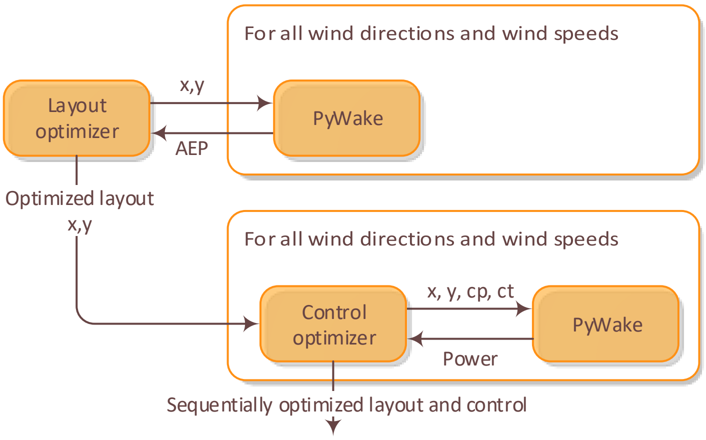

Figure 4. Sequential optimization workflow. The control settings are optimized one time only, after the optimal layout is found.

The merger of these two optimization steps ~~make~~makes up the optimized system design and is in essence a sequential application of the Topfarm2 (2019) layout platform and the open-loop WPP control scheduling platform described by ~~(~~Vitulli et al. (2019).

The layout is optimized using a combination of random search and gradient-based (SLSQP) optimization. The random search algorithm does not get stuck at local optima and is consequently suitable to find a good global solution, while the gradient-based optimizer, applied subsequently, is used to trim the random-search solution to the nearest optima. In this setup, the gradients are approximated by a finite difference approach. For a complex non-convex optimization problem, a global optimum cannot theoretically be ensured, but running numerous random sequences converging to almost identical results gives confidence to the result being close to the global optimum.

The WPP control scheduling optimization problem has in general only a few local optima and can therefore easily be solved by the gradient-based optimizer using gradients computed via finite difference. This control optimization is, however, rather time consuming, as the WT control settings must be optimized for all 360 x 23 combinations of wind directions and wind speeds; see ~~Table 1.~~Table 1. These combinations are, fortunately, independent, and the workflow therefore suitable for parallel computation. For the current study, a parallel workflow utilizing 360 CPUs (i.e. corresponding to a 1° mean wind direction resolution) has been ~~setup~~set up, where each CPU optimizes all WT control settings for one wind direction. Table 1 gives an idea of the computational resources needed for the case studies performed in ~~section~~Sect. ~~3~~9 and ~~section 4~~Sect.10.

	Row of 8 WT (1D layout, 1 WD, 23 WS)	Lillgrund, 48 WT, (2D layout, 360 WD, 23 WS)
PyWake, AEP calculation	0.002s	0.52s
Control optimization	3.5s	15h (1 CPU) 4 min (360 CPU)
Layout optimization	3.4s	2.8h (random search; 1 CPU) + 1.2h (gradient based; 1 CPU)

Table 1. Overview of time consumption of the AEP calculation, the control optimization and the layout optimization.

9. Sanity check

To check the overall behaviour of the optimizers, a sanity check on a simple illustrative example, consisting of a row with three Siemens SWT-2.3-93 WTs, has been performed. This case is selected, because it can be solved via ‘brute force’, and because the results are easily visualized.

9.1. Control optimization

The sanity check of the control optimization is performed on a simple example consisting of three WTs on a row, separated by 4*D*, ~~where *D* denotes the rotor diameter,~~ and with a uniform inflow of 10 m s^{-1} aligned with the row; see Figure 5.

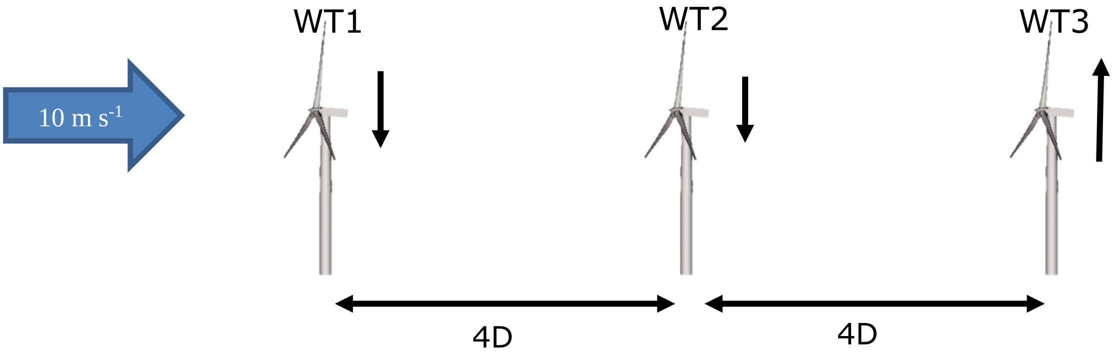

Figure 5. Three-WT row used for sanity check of the control optimization. **Reduced WT production, caused by derating, is indicated by an arrow pointing down - increased WT production, caused by optimized WPP control, is indicated by an arrow pointing upwards.**

Figure 6 shows the power produced by the three WTs as a function of the derating of the two upstream WTs. In the left plot, it is seen that the power for the most upstream WT, WT1, only depends on its own derating setting. The power of WT2, on the other hand, depends on the derating of both itself and of WT1. Finally, it is seen that WT3, obviously, produces the most, if both WT1 and WT2 ~~is~~are derated 100%.

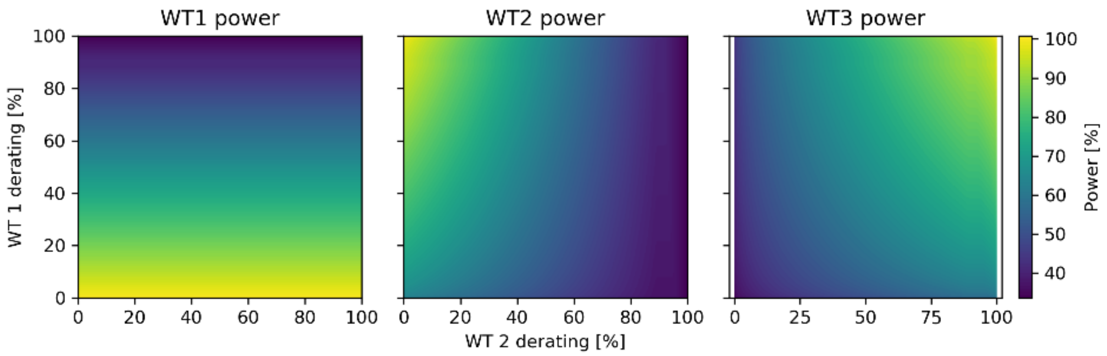

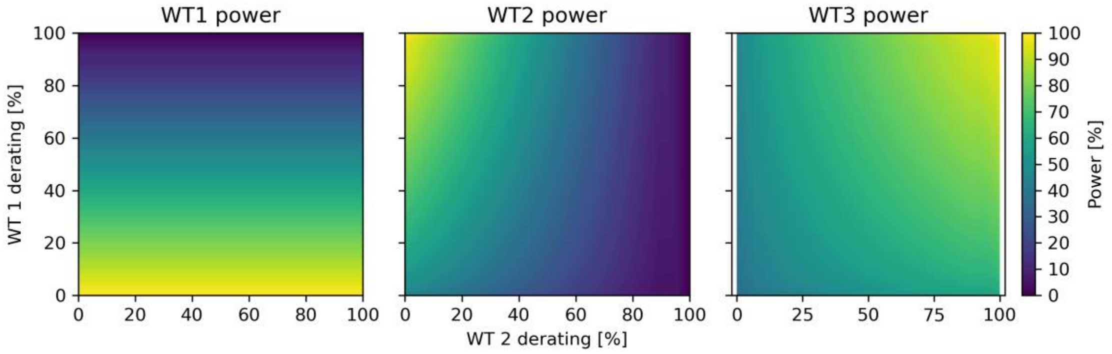

Figure 6. Power produced by the three WTs <u>in 10 m s^{-1}</u> as a function of WT1- and WT2 derating.

The total power produced by the three WTs is seen in Figure 7, and it appears that the total power can be increased by 4.01% if WT1 is derated by 7%, and WT2 is derated by 5%.

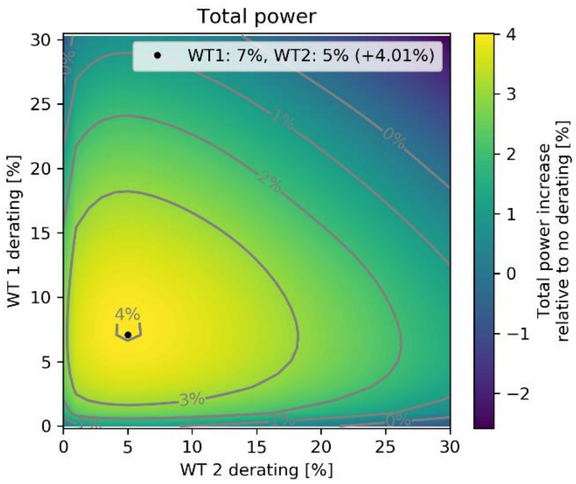

Figure 7. Total power of the three-WT row as a function of the derating of WT1 and WT2. The power can be increased by 4.01% when WT1 is derated by 7% and WT2 is derated by 5%.

9.2. Layout optimization

A sanity check of the layout optimizer is also performed on the three-WT row. In this case, the position of WT2 is allowed to vary between 2*D* and 6*D* behind WT1. Figure 8 shows the individual relative power production of the three WTs as well as the total power production as a function of the position of WT2 in a uniform flow of 10 m s^{-1} aligned with the row. As expected, WT1 is unaffected by the position of WT2, while the power production of WT2 increases with the distance to WT1, and vice versa for the power of WT3. Finally, the total power production is seen to increase slightly, when WT2 is moved downstream.

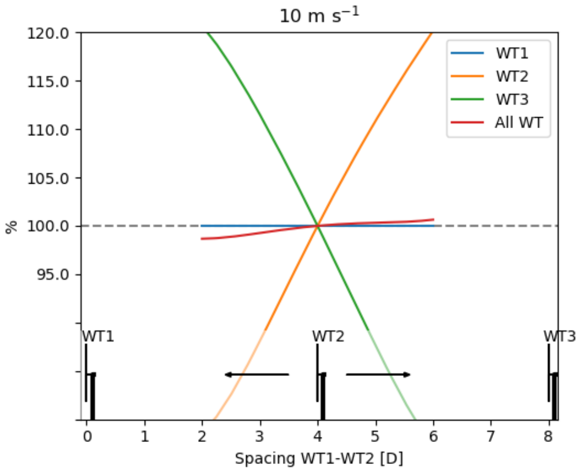

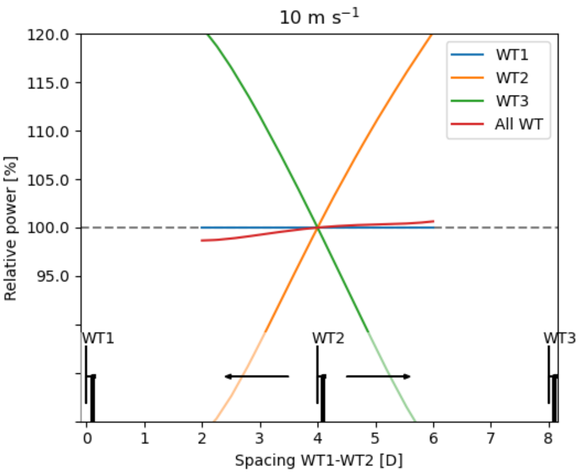

Figure 8. Relative power produced by the three individual WTs as well as the total relative power plotted as a function of the position of WT2.

For other wind speeds, however, the picture is quite different, as seen in Figure 9. The optimal position thereby depends on the wind speed distribution, which links to the ~~C_p and the C_t~~ dependence of C_p and C_t on wind speed with the hub-height mean wind speed. Plotting the relative AEP computed using the Weibull distribution associated with westerly winds at the Lillgrund wind farm (c.f. the wind rose shown in Figure 12) reveals, that the optimal spacing, under these conditions, is very close to 4*D*.

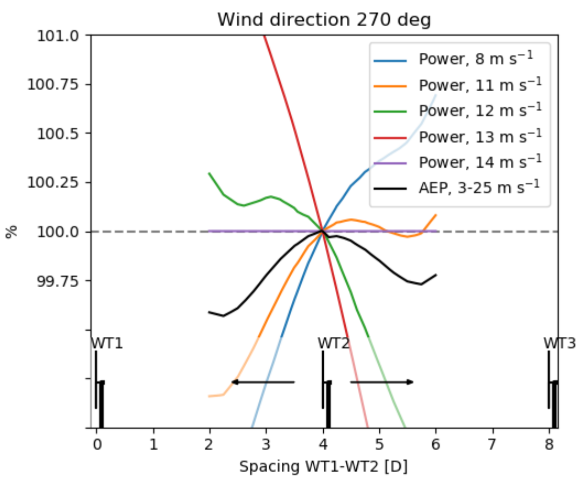

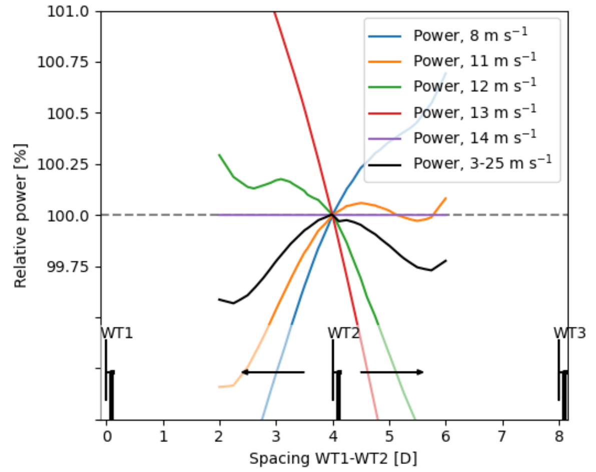

Figure 9. Relative total power production of the three WTs plotted as a function of the position of WT2 for different wind speeds. The power for 3-25 m s^{-1} is weighted by the Weibull distribution associated with wind from 270 °

9.3. Combined layout and control optimization

The performance of the integrated layout- and control optimization is illustrated in Figure 10. The blue line indicates the relative AEP of the three WTs as a function of the position of WT2 in case all WTs are operated 'greedy' (i.e. no derating). This is the base case. The optimal position of WT2 is found to be 3.96*D* downstream of WT1. Applying layout dependent optimal derating of WT1 and WT2 (orange curve) sequentially increases the AEP of the initial layout by 2.221%. Finally, the AEP is seen to increase only infinitesimally (i.e. increasing from +2.221% to +2.226%), when applying integrated *two-step nested* system optimization. For the investigated simplistic case, this result indicates a very weak system coupling between WPP ~~topology~~layout- and control optimization.

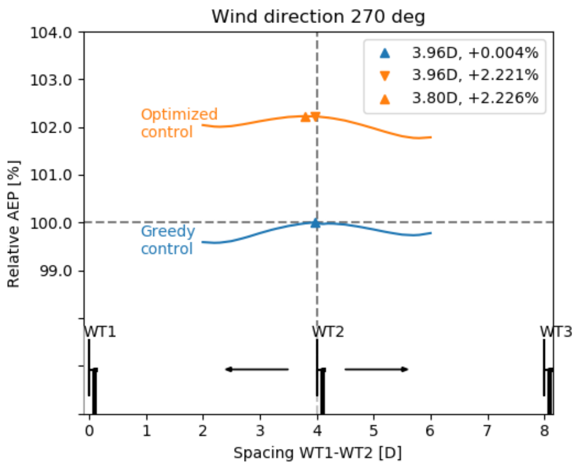

Figure 10. Relative AEP plotted as a function of the position of WT2 for both greedy and optimized control.

10. The Lillgrund showcase

The Lillgrund WPP is located in Øresund between Denmark and Sweden and consists of 48 Siemens SWT-2.3-93 WTs with a rotor diameter of 93 m. The WPP is known for its very small WT interspacings, down to 3.3*D* and associated pronounced wake effects. This makes this WPP especially suited for studies of WPP performance. The WPP layout is shown in Figure 11.

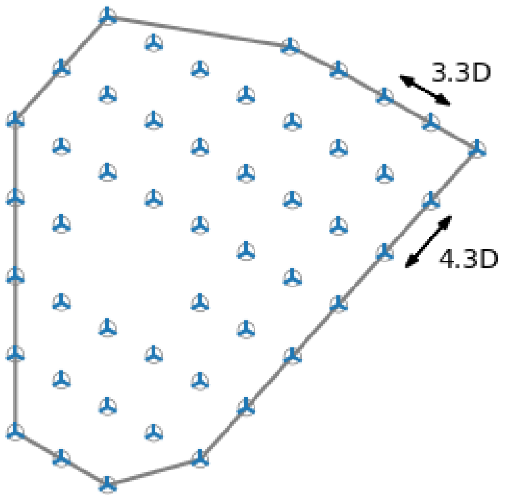

Figure 11. WT positions in the offshore Lillgrund WPP.

The Lillgrund wind climate is outlined in Appendix A in terms of ambient mean wind speed pdfs (i.e. two-parameter Weibull), conditioned on the ambient mean wind direction as well as an ambient mean wind direction pdf. For the sake of illustration, the applied wind climate information is condensed in the wind rose shown in Figure 12, which reveals predominant winds from west and south.

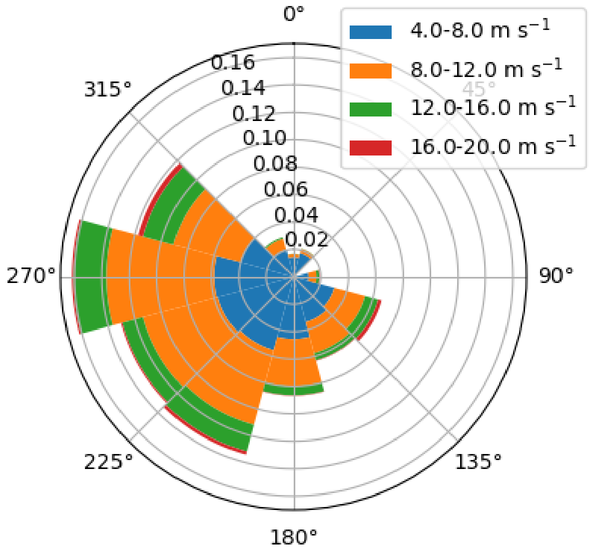

Figure 12. Wind rose characterizing the wind climate at the Lillgrund wind farm. Mean wind speed bins are shown in different colours, and their occurrence probabilities (conditioned on the respective inflow sectors) are proportional to their respective radial extend.

First, we will focus on a subset of the Lillgrund WPP consisting of a row of eight WTs with along-row inflow conditions covering the entire relevant wind speed regime – i.e. the wind speed regime within which these WTs are in normal operation. Using this simplified case study, we will investigate the system coupling between WPP ~~topology~~layout- and WPP control optimization. Based on the results from this study, we will next perform a system optimization of the Lillgrund WPP and thereby quantify its potential in terms of increased AEP compared to the base case, which is the present layout (cf. ~~Figure 11~~Figure 11) without coordinated WPP control – i.e. only conventional 'greedy' control of the individual WTs.

10.1. Eight-WT row

This case study basically consist of one of the three Lillgrund WWP rows with eight WTs, meaning that the WT interspacing in the base case is 3.3*D* (cf. Figure 11), and that the WTs are Siemens SWT-2.3-93. The wind climate is fictitious, as only an along row inflow direction is considered, which assures largest possible mutual WT wake interactions. Within this framework we have, without loss of generality, assumed Weibull distributed mean wind speeds corresponding to the 270° site condition (however, truncated to the relevant wind speed regime [3 m s^{-1}; 25 m s^{-1}]) although the 'true' inflow direction associated with this row is 300°.

With the purpose of investigating the strength of the system coupling, we have optimized: 1) the WPP ~~topology~~layout; 2) the WPP control; 3) the integrated WPP ~~topology~~layout and WPP control based on the *two-step sequential* approach (cf. ~~section~~Sect. 8.4); and 4) the integrated WPP ~~topology~~layout and WPP control based on the *two-step nested* approach (cf. ~~section~~Sect. 8.4). Based on a pre-investigation of optimizers, where the 'random search' approach was compared to the SLSQP gradient-based optimization algorithm, the latter was found clearly superior and consequently used in this study.

The results of the investigation are, together with the base case (0), summarized in Table 2.

Case	Layout	Control	AEP [Gwh]	CPU time [s]	
0	Initial	Greedy	40.85	0.01	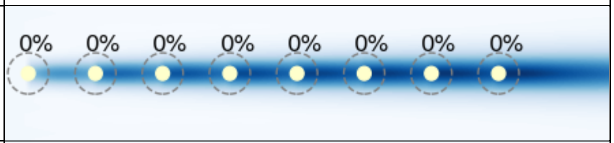
1	Initial	Optimized	44.10 (+8.0%)	4.20	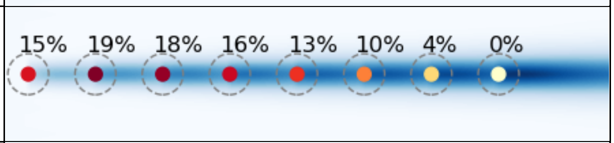
2	Optimized	Greedy	41.44 (+1.4%)	2.84	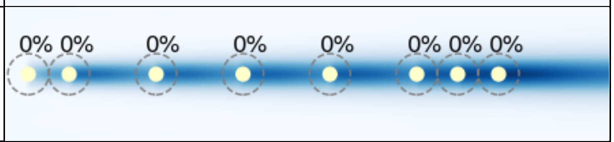
3	Optimized	Optimized (sequential)	44.558 (+9.1%)	6.92	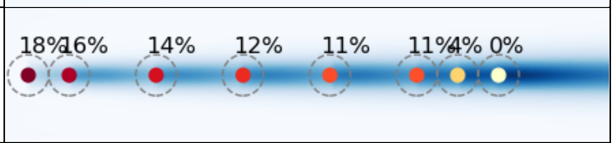
4	Optimized	Optimized (nested)	44.560 (+9.1%)	3731	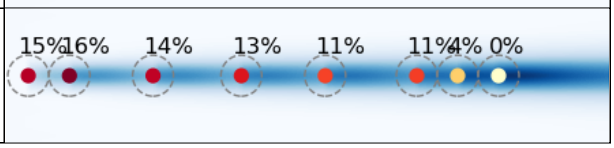

Table 2. AEP results of various optimization approached applied on the eight-WT row. The CPU times refer to the computation time on a standard laptop PC. The figures in the rightmost column show the position of the eight turbines. The derating settings of the WTs are indicated by the colour of the turbine symbol and quantified in percentage by the number above the WT symbols.

The base case, case(0), represents the existing layout with conventional greedy control of the individual WTs. Case(1) represents the base case ~~topology~~layout with the WPP control optimized. The associated increase in AEP, relative to the base case, is significant and amounts 8.0%. ~~In case(2) the WT applies greedy control, and the WT row topology is optimized. The increase in AEP, relative to the base case, amounts to 1.4%, which is considerable less than achieved in case(1).~~The close spacing in the Lillgrund WPP case (3.3*D*) is comparable with the WT inter spacing (2.3*D* - 3.1*D*) in the Goole Fields WPP investigated in (van der Hoek et al., 2019), where an increase of 5.6% for a row of five WTs was predicted, and an increase of 3.3% was realized in the accompanying full-scale study. As noted in the discussion of the results in this paper, the *k-ε* turbulence closure of the CFD model, which was used for tuning of the derating settings, supposedly makes the CFD predictions underestimate wake effects for closely spaced WTs, whereby the used pitch settings are likely to be sub-optimal.

Furthermore, only the first WT in the investigated row was derated, their two-step pitch-offset derating strategy was suboptimal, and finally the derating potential increases with the number of WTs. This, paired with the fact that full-scale studies always will suffer from imperfect inflow (wind direction variability within the 10-minute recording sequences etc.) and WT operational conditions (moderate yaw errors etc.) make us believe that the case(1) result is fairly consistent with the results presented in (van der Hoek et al., 2019). In case(2) the WT applies greedy control, and the WT row layout is optimized. The increase in AEP, relative to the base case, amounts to 1.4%, which is considerably less than achieved in case(1). Compared to the three-WT case in Figure 10, the AEP increase achieved by layout optimization in this case is much more pronounced because the number of design variables has increased from one to six. It is seen that the distance between the two most upstream and the tree most downstream WTs are smaller than in the base case. This allows larger spacing and thereby production of the middle turbines, which, in this case, results in an increase of the AEP of the whole row. Obviously, this strategy is not possible with only three WTs. Case(3) represents one of two system optimization approaches. Here we assume that the system optimization is separable and consequently can be performed by first optimizing the ~~topology~~layout and subsequently the WPP control. The combined effect is an increase in AEP amounting to 9.1%, which is significant and exceeds what was obtained by only optimizing the WPP control (i.e. case(1)). In the second and last system optimization strategy, case(4), ~~a~~ the integrated *two-step nested* approach is taken. Although being more complex and time consuming (around 540 times slower) than the case(3) strategy, the outcome is ~~only *insignificantly*~~not significantly improved (cf. Table 2).

In conclusion, we have shown that the strength of the system coupling between WPP ~~topology~~layout- and WPP control optimization is only marginal for the considered eight-WT case study characterized by 'heavy' mutual WT wake interactions.

10.2. Full Lillgrund wind farm

This case study comprises the entire Lillgrund WPP, and it eventually aims at quantifying the potential of an integrated system optimization of WPP ~~topology~~layout and WPP control.

In analogy with ~~section~~Sect. 10.1, we will investigate a variety of WPP ~~topology~~layout and WPP control optimization strategies. The control optimization schedule and the associated results appears from Table 3.

Case	Layout	Control	AEP [Gwh]
0	Initial	Greedy	345.2
1	Initial	Optimized	349.5 (+1.3%)
2	Optimized	Greedy	354.9 (+2.8%)
3	Optimized	Optimized(sequential)	358.7 (+4.0%)
~~4~~	~~Optimized~~	~~Optimized(nested)~~	~~-~~

Table 3. AEP results of various optimization approached applied on the full Lillgrund WPP.

The investigated cases are ~~analogue~~analogous to the cases investigated for the eight-WT case in ~~section~~Sect. 10.1. As for case(1) we see a ~~considerable~~considerably drop in performance increase compared to the eight-WT situation, which is due to the persistently more severe mutual WT wake interactions in the fictitious eight-WT situation compared to the full Lillgrund WPP, where WT wake interactions for some inflow directions are limited (cf. Figure 14). With less wake interaction follows intuitively less potential for WPP control. Case(2) represent an isolated WPP layout optimization retaining the 'greedy' individual WT control performance. The associated increase in AEP performance amounts to 2.8% – or more than ~~doubled compared to~~double that of the WPP control optimization, case(1). The last case, case(3), represents a system optimization approach. Based on the investigations performed in both ~~section~~Sect. 9.3 and ~~section~~Sect. 10.1, we assume that the system optimization is separable in the sense described in ~~section~~Sect. 10.1. The rationale justifying this assumption is, that the system coupling between WPP ~~topology~~layout- and WPP control optimization was shown to be marginal in the eight-WT case, in which the overall WT wake interaction, over all inflow directions, are significantly more pronounced than for the full Lillgrund case. Taking the sequential approach, the combined Lillgrund WPP optimization results in an AEP improvement of 4.0%, which is significantly more than each of the individual ~~topology~~layout and WPP control optimization approaches. Finally, it should be noted that, although possible, the *two-step nested* approach will require horrendous CPU resources and even on a cluster take in the order of a few months to conduct.

The layout resulting from the Lillgrund WPP system optimization is shown in Figure 13 together with the base line layout.

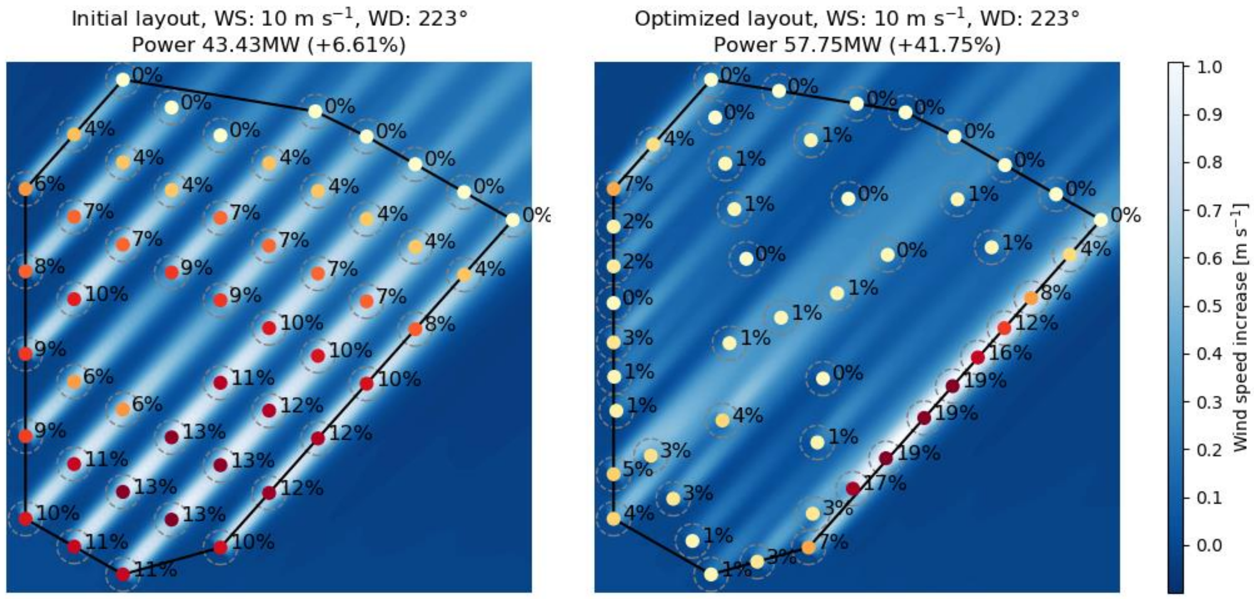

Figure 13. The base line Lillgrund WPP layout (left) and optimized Lillgrund WPP layout (right). The two figures show the flow case associated with 10 m s^{-1} inflow from direction 223°. The derating settings of the individual WTs are indicated by the colour of the WT symbols and quantified in percentage by the number above the WT symbols. The background colours illustrate the increase in wind speed from the individual 'greedy' to the 'collaborative' optimized control situation.

From a pure production perspective, it makes sense to locate WTs densely at the boundary of the 'admitted area' for the WPP, because it intuitively will reduce the WT wake interactions. Notable is also that the individual WT deratings for the shown example, except for one row, is considerable less than for the base line case.

The results for all the investigated optimization strategies are summarized in Figure 14 and Figure 15. Figure 14 shows the increase in AEP conditioned on the inflow mean wind direction. As expected, the AEP gains vary with the wind direction with huge increases, up to 50%, for the optimized layout for the wind directions that is parallel to the rows of the original layout, i.e. 120°/300°, 42°/222° and 0°/180°. These increases, however, are almost balanced out by the decrease at other directions resulting in the average increase of the 2.8% and 4% increase that is reported in Table 3.

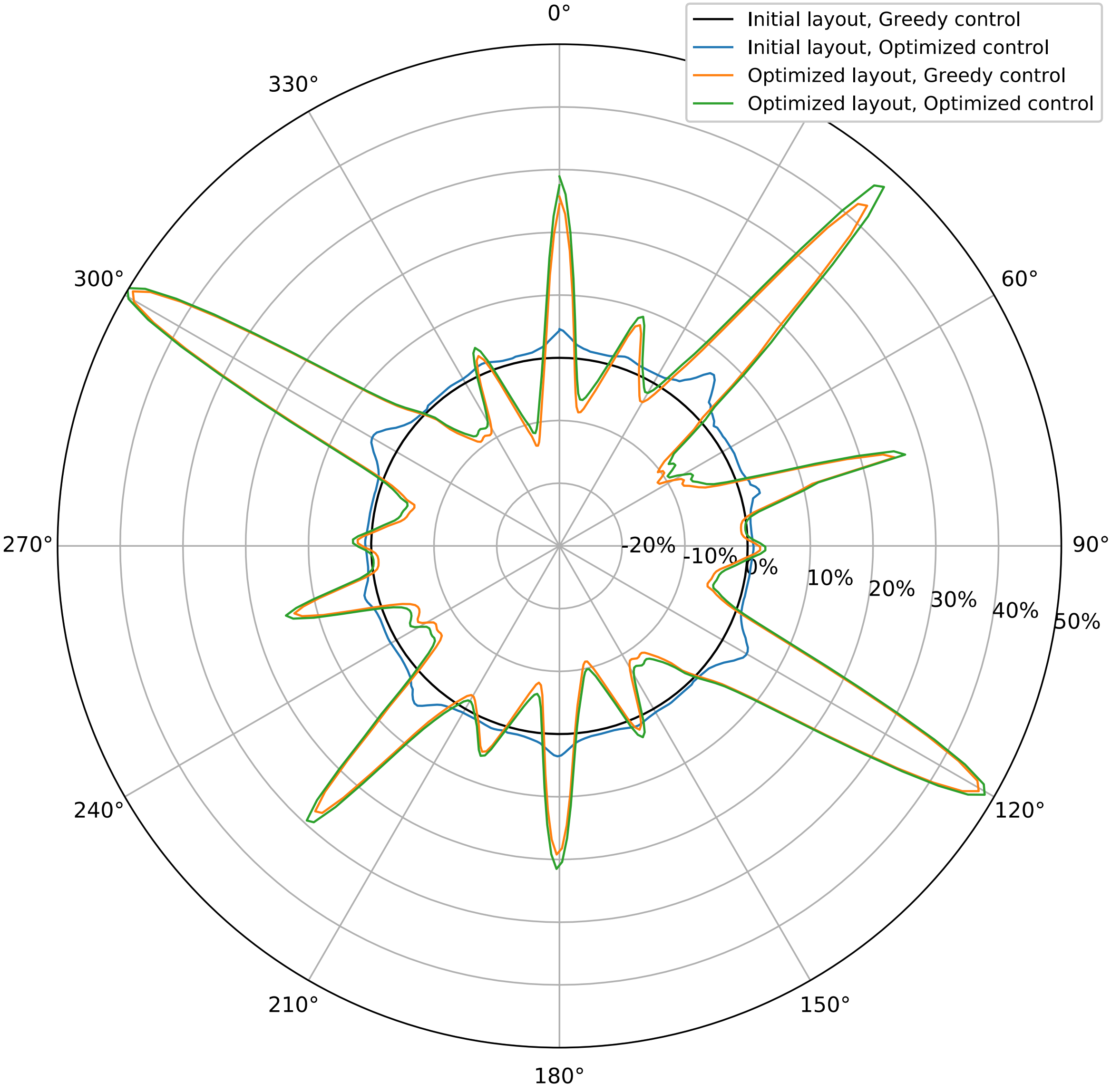

Figure 14. Increase in AEP due to layout and/or control optimization plotted as a function of inflow wind direction.

In Figure 15, the AEP gains are shown as a function of the mean inflow wind speed. The largest increases are seen below 10-11 m s^{-1} where all WTs operate below rated power. At higher wind speed, the WPP production wake losses decreases, as more and more WT reaches rated power, thus eventually completely eliminating any WPP control potential.

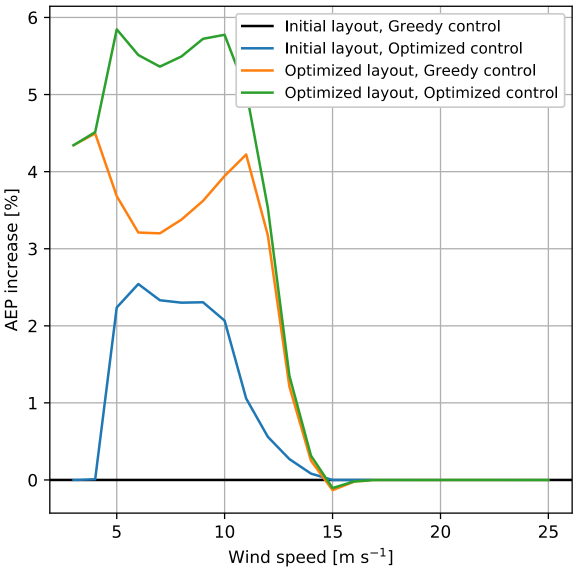

Figure 15. Increase in AEP due to layout and/or control optimization plotted as a function of wind speed.

11. Conclusions

This paper describes a platform for integrated WPP ~~topology~~layout- and derating-based WPP-control optimization. The objective function for the optimization is the AEP of the WPP without considering financial costs of internal WPP grid etc. This means that the positions of the individual WPP WTs are only constrained by a minimum allowable distance to the nearest neighboring WT, in this case 2D, and the convex boundary around the initial WPP layout.

~~-~~As WPP loading is excluded, stationary modeling of the complex WPP flow field suffices, which is a considerable simplification. Contrary to other known WPP optimization platforms, the present approach is based on a consistent and very fast CFD solver, whereby the ~~inherit~~inherent uncertainties associated with simple empirical algebraic wake models, including their often debatable wake summation 'receipt', is avoided. This strategy is consistent with a recent review of WPP optimization approaches (Kheirabadi and Nagamune, 2019), where one of the conclusions is that "*added layers of realism in terms of simulated wind conditions tend to deteriorate the performance of wind farm controllers*", thus stressing the importance of carefully and realistically simulated WPP flow fields.

The platform has initially successfully been subjected to a simplistic sanity check. Subsequently, the platform has been used to analyze the potential of an integrated WPP ~~topology~~layout and WPP control optimization of the offshore WPP Lillgrund, which consists of 48 closely spaced WTs. ~~Introductory~~First, an analysis of the system coupling between WPP ~~topology~~layout optimization and WPP control optimization is performed as based on a subset of this WPP exposed to inflow conditions clearly exaggerating the overall complex inter-WT aerodynamic interactions within a traditional WPP~~.~~, because all the WTs are in a state of maximum wake interaction. The study demonstrates an inferior system coupling only, thus justifying separation of the present optimal system design. Based on this learning, a full system optimization of the Lillgrund WPP is performed, resulting in a gain amounting to 4.0% in AEP relative to the base line case, which is the present Lillgrund layout without WPP control. In a future perspective, the platform will be extended to also include active wake control in terms of WT yaw dictated wake deflection. This requires a generalization of the applied linearized CFD flow solver Fuga – a work that is in progress.

12. Data availability

Simulation data not available due to confidentiality of the Siemens WT model.

13. Author contribution

GCL has designed the numerical study. MMP implemented and run the optimizations. The paper was written and reviewed in cooperation.

14. Competing interests

The authors declare that they have no conflict of interest.

15. Acknowledgement

Financial support from the EU Horizon 2020 research and innovation program, under grant agreement no. 727680 (TotalControl), is acknowledged. Siemens ~~Wind Power~~Gamesa Renewable Energy is acknowledged for making the aerodynamic data of the Siemens SWT-2.3-93 WT available for the Lillgrund study.

16. References

S. J. Andersen. A Comparative Study of the Wake Dynamics during Yaw and Curtailment. Zenodo. http://doi.org/10.5281/zenodo.3357798. (2019)

A. P. Deshmukh and J. T. Allison. Unrestricted wind Farm Layout Design with Optimal Control Considerations. Proceedings of the ASME 2017 International Design Engineering Technical Conferences and Computers and Information in Engineering Conference, IDETC/CIE 2017, August 6-9, Cleveland, Ohio, USA. (2017)

H. K. Fathy, J. A. Reyer, P. Y. Papalambros and A. G. Ulsoy. On the Coupling Between the Plant and Controller Optimization Problems. 2001 American Control Conference, Vol. **3**, pp. 1864–1869. (2001)

P. A. Fleming, A. Ning, P. M. O. Gebraad and K. Dykes. Wind plant system engineering through optimization of layout and yaw control. Wind Energy, **19**, pp. 329– 344. doi: 10.1002/we.1836. (2016)

P. M. O. Gebraad, P. A. Fleming and J. W. van Wingerden. Comparison of actuation methods for wake control in wind plants. American Control Conference, Chicago, USA. (2015)

P. M. O. Gebraad, J. J. Thomas, A. Ning, P. A. Fleming and K. Dykes. Maximization of the annual energy production of wind power plants by optimization of layout and yaw-based wake control. Wind Energy, **20**, pp. 97– 107. doi: 10.1002/we.1993. (2017)

T. Göçmen and G. Giebel. Estimation of turbulence intensity using rotor effective wind speed in Lillgrund and Horns Rev-I offshore wind farms. Renew. Energy, **99**, pp. 524–532. doi:10.1016/J.RENENE.2016.07.038. (2016)

J. S. Gray, J. T. Hwang, J. R. R. A. Martins, K. T. Moore, and B. A. Naylor, "OpenMDAO: An Open-Source Framework for Multidisciplinary Design, Analysis, and Optimization," Structural and Multidisciplinary Optimization, 2019.

M. H. Hansen, L. C. Henriksen, C. Tibaldi, L. Bergami, D. Verelst and G. Pirrung. HAWCStab2 User Manual. DTU Wind Energy. (2017)

D. van der Hoek, S. Kanev, J. Allin, D. Bieniek and N. Mittelmeier. Effects of axial induction control on wind farm energy production - a field test. Renew. Energy 140, pp. 994–1003. https://doi.org/10.1016/j.renene.2019.03.117. (2019)

N. O. Jensen. A note on wind generator interaction. Risø-M-2411, Risø National Laboratory,Roskilde. (1984)

A. C. Kheirabadi and R. Nagamune. A quantitative review of wind farm control with the objective of wind farm. Journal of Wind Engineering & Industrial Aerodynamics, **192**, pp. 45–73. (2019)

van der Laan, M. P., Andersen, S. J., Ramos García, N., Angelou, N., Pirrung, G. R., Ott, S., Sjöholm, M., Sørensen, K. H., Vianna Neto, J. X., Kelly, M., Mikkelsen, T. K., and Larsen, G. C.: Power curve and wake analyses of the Vestas multi-rotor demonstrator, Wind Energ. Sci., 4, 251–271, https://doi.org/10.5194/wes-4-251-2019, 2019.

G. C. Larsen, P.-E. Réthoré. TOPFARM – A Tool for Wind Farm Optimization. Energy Procedia, vol. **35**, pp. 317–324. (2013)

E. Machefaux, G. C. Larsen, N. Troldborg, M. Gaunaa and A. Rettenmeier. Empirical Modelling of Single Wake Advection and Expansion using Full Scale Pulsed Lidar based Measurements. Wind Energy, **18** (12), pp. 2085–2103. (2015)

H. Aa. Madsen, R. Mikkelsen, N. N. Sørensen, M. L. O. Hansen, S. Øye and J. Johansen. Influence of wind shear on rotor aerodynamics, power and loads. Research in Aeroelasticity EFP-2006, Risø-R-1611(EN). (2007)

S. Mahulja, G. C. Larsen and A. Elham. Engineering an optimal wind farm using surrogate models. Wind Energy. Vol. **21**, Issue12, pp. 1296-1308. (2018)

S. Ott, J. Berg and M. Nielsen. Linearised CFD Models for Wakes. Risoe-R-1772(EN). (2011)

Peña, A., Schaldemose Hansen, K., Ott, S., and van der Laan, M. P.: On wake modeling, wind-farm gradients, and AEP predictions at the Anholt wind farm, Wind Energ. Sci., 3, 191–202, https://doi.org/10.5194/wes-3-191-2018, 2018.

PyWake. https://doi.org/10.5281/zenodo.2562662. (2019)

P.-E. Réthoré, P. Fuglsang, G. C. Larsen, T. Buhl, T. J. Larsen and H. Aa. Madsen. TOPFARM: Multi-fidelity optimization of wind farms. Wind Energy, vol. **17**, pp. 1797–1816. (2013)

Topfarm2. https://doi.org/10.5281/zenodo.3247032. (2019)

J. A. Vitulli, G. C. Larsen, M. M. Pedersen, S. Ott~~,~~ and M. Friis-Møller. Optimal open loop wind farm control, J. Phys. Conf. Ser., 1256, 12027, doi:10.1088/1742-6596/1256/1/012027. (2019)

Appendix A

Wind sector (centered) [deg]	Frequency [%]	Weibull scale (A)	Weibull shape (k)
0	3.8	4.5	1.69
30	4.5	4.7	1.78
60	0.4	3.	1.82
90	2.8	7.2	1.7
120	8.3	8.8	1.97
150	7.5	8.2	2.49
180	9.9	8.4	2.72
210	14.8	9.5	2.7
240	14.3	9.2	2.88
270	17.	9.9	3.34
300	12.6	10.3	2.84
330	4.1	6.7	2.23

Table 4. Sector probability and Weibull shape and scale parameters for the Lillgrund site. Data obtained from the study of Göçmen and Giebel (2016)